JOURNAL OF GEOPHYSICAL RESEARCH, VOL. 106, NO. B11, PAGES 26,311–26,329, NOVEMBER 10, 2001

Fluid flow patterns in fast spreading East Pacific Rise crust exposed at Hess Deep

Kathryn M. Gillis,[1] Karlis Muehlenbachs,[2] Michael Stewart,[3]
Thomas Gleeson,[1] and Jeffrey Karson[3]

Abstract. Tectonic exposures of a volcanic sequence and sheeted dike complex over a 4-km-wide region at Hess Deep (equatorial Pacific) reveal significant spatial heterogeneity (10–10^3 m) in the extent and nature of hydrothermal alteration in young, fast spreading East Pacific Rise crust. The volcanic sequence is fairly uniformly altered, with only minor oxidation and alteration to clay minerals. Sheeted dikes in the eastern part of the field area are highly fractured with narrow intervals of intact dikes that dip up to 60°. Their alteration characteristics show a simple depth trend such that with increasing depth the dominant secondary mafic mineral changes from chlorite to amphibole, clinopyroxene replacement increases (<20% to >40%), whole rock $\delta^{18}O$ values decreases (4.4–5.5‰ to 3.5–4.5‰), and calculated peak metamorphic temperatures increase (~250°C to 450°–700°C). Within the deepest dikes, localized zones up to 400-m-wide are chlorite-rich and have low-$\delta^{18}O$ (2.9–4.1‰) and low peak metamorphic temperatures (~345°C). These alteration patterns likely formed within broad recharge zones whereby the low-$\delta^{18}O$ zones developed in the regions with the highest fluid flux. In the west, massive, slightly rotated sheeted dikes near the volcanic–sheeted dike transition are $\delta^{18}O$ and Cu depleted and display higher peak temperatures (≥345°C) than elsewhere in the shallow dikes. These characteristics are consistent with formation within a high temperature, hydrothermal discharge zone. We propose that the spreading history of a fast spreading ridge segment can create significant spatial heterogeneity in fluid flow and alteration patterns within sheeted dike complexes, similar to those preserved in many ophiolites.

1. Introduction

Alteration of the oceanic crust by seawater is of fundamental importance to many global geochemical cycles [e.g., *Bischoff and Dickson*, 1975; *Staudigel et al.*, 1996; *Thompson*, 1983; *Wolery and Sleep*, 1976]. Hydrosphere–lithosphere interaction must be heterogeneous over time and space, but detailed study of the crustal component of these systems has been limited because of sparse drill core samples and dredged samples of unknown field relationships. What goes on within the crust during vigorous hydrothermal circulation has largely been inferred from vent fluid chemistry [e.g., *Von Damm*, 1995] and heat flow measurements [e.g., *Baker et al.*, 1996], with theoretical and experimental approaches providing the links to altered rocks (see review by *Saccocia et al.* [1994]). Conceptual models for fluid-rock interaction in hydrothermal cells emphasize depth-related trends such that fluid flows down into the crust within broad recharge zones and rises to the seafloor in focused zones of discharge. An increase in temperature coupled with a decrease in permeability along the recharge pathway leads to predictable mineralogical and geochemical changes to the crust. At the base of the hydrothermal system, which would be centerd at the sheeted dike–plutonic sequence at fast spreading ridges, hydrothermal fluid compositions are thought to become fixed prior to their ascent to the seafloor.

Hydrothermal alteration patterns documented for many ophiolites show that there can be much more spatial heterogeneity in alteration patterns within the oceanic crust than would be expected from conventional mid-ocean ridge (MOR)-based models. Early regional-scale investigations emphasized the importance of depth-related trends in features such as alteration mineralogy, degree of alteration, and bulk rock compositions (e.g., O and Sr isotopic ratios), which reflect the combined effects of changing lithology, increasing temperatures, and decreasing water/rock ratios [e.g., *Elthon et al.*, 1984; *Gregory and Taylor*, 1981; *Harper et al.*, 1988; *McCulloch et al.*, 1981]. Subsequent studies have documented significant lateral heterogeneities in alteration characteristics that are linked to the particular magmatic and structural evolution of each ophiolite [e.g., *Alexander et al.*, 1993; *Lécuyer and Fourcade*, 1991; *Nehlig and Juteau*, 1988; *Stakes and Taylor*, 1992].

It is a challenging task to test predictions about subsurface processes because our collections of hydrothermally altered rocks record the time-integrated effects of fluid-rock interaction, not the near instantaneous view of active vents. Moreover, the specific history of tectonic and magmatic activity for a ridge segment, which is strongly linked to hydrothermal processes [*Haymon et al.*, 1991], is generally not known for our rock collections. Extensive field studies of fast spreading ridges show that vigorous high temperature hydrothermal activity that leads to the accumulation of sulphides at the seafloor is not prevalent everywhere along a ridge segment [e.g., *Hooft et al.*, 1997]. Moreover, the life cycle of East Pacific Rise (EPR) vent sites is of the order of tens to hundreds of years [*Von Damm*, 1995] because they are

[1]School of Earth and Ocean Sciences, University of Victoria, Victoria, Briitsh Columbia, Canada.
[2]Department of Earth and Atmospheric Sciences, University of Alberta, Edmonton, Alberta, Canada.
[3]Division of Earth and Ocean Sciences, Duke University, Durham, North Carolina, USA.

Paper number 2000JB000038.
0148-0227/01/2000JB000038$09

either buried by lava or changes in the hydrological and thermal structure of the crust occur [*Curewitz and Karson*, 1998]. This means that fluid-rock interaction in many areas along a ridge segment does not necessarily evolve within an "ore-forming" system.

In this paper we document the spatial and temporal variability in hydrothermal processes recorded in a 4-km-wide tectonic exposure of volcanic rocks and sheeted dikes that formed at the fast spreading EPR. These exposures provide a unique window to map on an outcrop scale the field relationships of differently altered crust and gain insights into the "plumbing" of hydrothermal systems. Mineralogical and geochemical characteristics and whole rock O isotope data for samples recovered along 14 submersible dive tracks reveal complex alteration patterns and identify fluid flow pathways. We use these new data to evaluate the spatial and temporal scales of variability in the crustal component of oceanic hydrothermal systems.

2. Geological Background

2.1. Tectonic Setting and Geological Relationships

The western end of the Cocos-Nazca spreading center is propagating into the eastern side of the Galapagos microplate, rifting young (0.5–1.2 Ma) crust that was generated at the fast spreading (130 mm/yr) EPR [*Lonsdale*, 1988]. The present EPR axis forms part of three plate boundaries (Pacific-Nazca, Pacific-Cocos, and Pacific-Galapagos microplate). Bathymetric and magnetic data from the western flank of the EPR indicate that the crust being rifted at Hess Deep is an amalgamation of crustal blocks that formed either in-place or were transferred from these axes [*Lonsdale*, 1999]. Middle to upper crustal sections composed of in-place crust that accreted at the Pacific-Nazca ridge and are typical of the fast spreading EPR are exposed along east–west trending scarps that bound the rift valley [*Francheteau et al.*, 1990; *Lonsdale*, 1999].

This report focuses on a portion of a rift shoulder horst that is located on the northern scarp of the rift valley where ~1.2 Ma EPR crust is exposed (Figure 1). Fourteen dives conducted during two *Alvin* dive programs (1990, 1999) investigated a 4-km-wide area which records ~60,000 years of spreading history, with units younging from west to east (Figure 2a). Volcanic rocks form the crest of the horst and grade downslope (to the south) into the sheeted dike complex, followed by the uppermost plutonic sequence (see inset in Figure 2a for cross section) [*Karson et al.*, 1992; 2001]. In this 4-km-wide area, the thickness of the volcanic sequence increases (from <200 to >600 m) and the depth of the volcanic–sheeted dike transition deepens (from ~2000 to 2500 m below sealevel (bsl)) from west to east. The sheeted dike complex is ~500 m thick and consists of individual dikes or packets of subparallel dikes dipping to the east at an average dip of 60°, and in localized areas are highly fractured. Gabbroic rocks crop out at depths greater than ~3000 mbsl (Figure 2) and the gabbro–sheeted dike transition is marked by a narrow zone of intercalated dikes and gabbros.

2.2. Alteration Patterns

The alteration characteristics of the volcanic sequence and sheeted dike complex demonstrate that hydrothermal alteration patterns are spatially complex and do not vary simply with depth (e.g., Ocean Drilling Program (ODP) Hole 504B [*Alt et al.*, 1996]). In order to introduce these complexities we first subdivide the rift shoulder horst region into two areas and describe their general geological relationships (summarized from P. Lonsdale (unpublished cruise data, 1990), *Karson et al.* [1992], J.A. Karson et al. (unpublished cruise report, 1999), *Karson et al.* [2001]) and alteration characteristics.

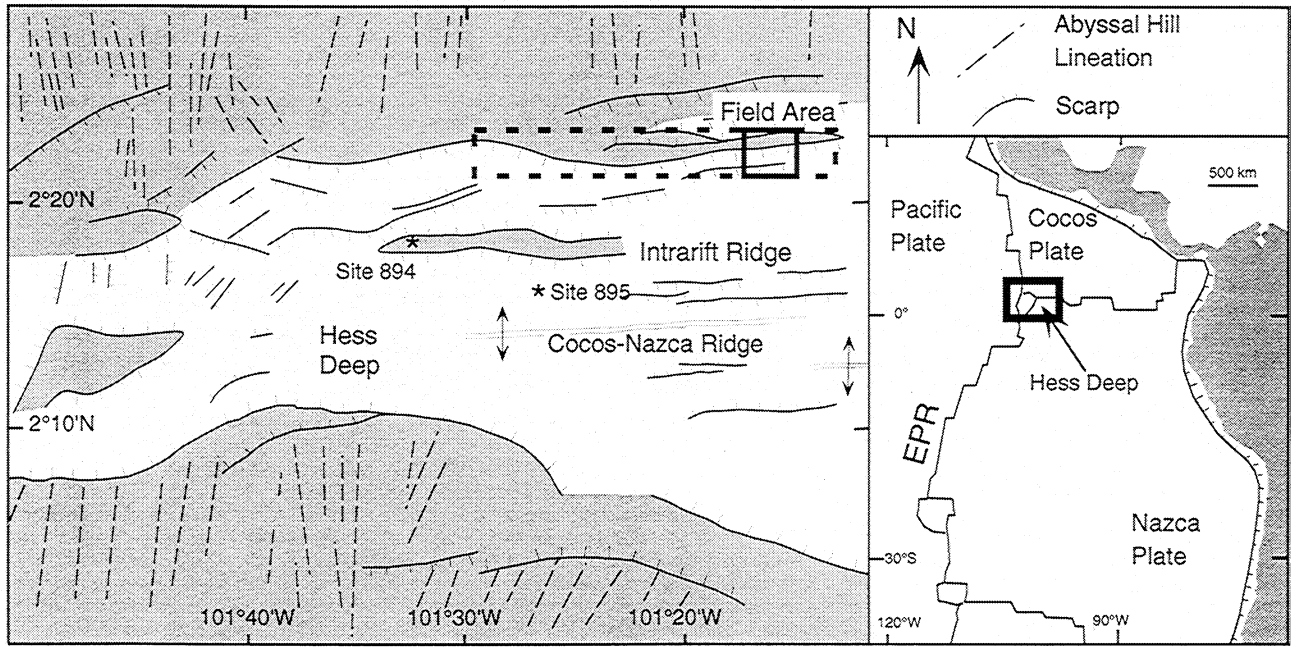

Figure 1. Location and schematic tectonic maps of the Hess Deep area [after *Lonsdale*, 1988]. Gray denotes regions of crust that were generated at the axis of the East Pacific Rise and have north-south oriented abyssal hill lineations. The solid box identifies the field area for this study where *Alvin* dives were conducted in 1990 and 1999. The dashed box shows the area investigated during the 1999 field program, which included a DSL-120 side-scan sonar survey, and Argo photographic surveys and *Alvin* dives in selected areas [*Karson et al., in press*].

Area 1 is located in the western part of the field area and includes dives that explored both the northern (dive 2216) and southern (dives 2214, 3373) slopes of the rift shoulder horst (Figure 2a). Here, the volcanic sequence is thin (~200 m), and samples show minor oxidation, enrichment in Rb, K_2O, and $\delta^{18}O$ relative to fresh rock values, and little or no alteration to clay minerals. In area 1, the sheeted dike complex is exposed between ~2000 m and 2250 mbsl. Individual dikes are intact and weakly jointed and dip steeply (~80°) to the east. Dike samples show moderate replacement of clinopyroxene by chlorite or amphibole, significant O isotope depletion (as low as 2.7‰), and many samples are depleted in metals (i.e., Cu <30 ppm). A mineralized fault zone along dive 2214, interpreted as a fossil hydrothermal upflow zone [*Saccocia and Gillis*, 1995], is the only evidence for high-volume hydrothermal flow. At depths >2250 mbsl (dive 3373) the lithology changes to a mixed zone of dikes and volcanics (note that this part of the dive is denoted as sheeted dikes in Figure 2). Samples from these depths show the same alteration characteristics as the volcanic sequence.

Area 2 extends to the east of area 1and encompasses the rest of the field area. Here, the volcanic sequence is 500–700 m thick and grades downward into a mixed assemblage of dikes and volcanics that lie above the sheeted dike complex (Figure 2a). The region between the 2000 and 2500 m contours is composed of volcanics with a few narrow zones of high-level dikes (dives 2217 and 3368). The upper third of the volcanic sequence is composed of intact pillows and lesser lobate flows, whereas the lower two thirds is intensely fractured and locally cut by basaltic dikes. Similar to area 1, volcanic samples show minor oxidation, enrichment in Rb, K_2O, and $\delta^{18}O$ with the greatest enrichment occurring in the fractured areas, and little or no alteration to clay minerals. At ~2500 mbsl, outcrops become dominantly sheeted dikes with localized volcanic screens (dives 3366 and 3375). Outcrops are commonly highly fractured with narrow intervals of intact dikes that dip ~60° to the east. These uppermost, sheeted dikes are slightly to moderately altered, chlorite ± minor amphibole is the dominant secondary mineral, most samples show no metal mobilization, and O isotope values range from 4.6 to 5.5‰. At deeper levels in the sheeted dikes (dives 3367, 2212, 2213, 2215) the dikes show the same degree of localized fracturing and dike rotation as at shallower depth but recovered samples show considerable variation in their alteration characteristics. At the intersection of dives 2215 and 3366 (SW end of dives), samples from an ~400-m-wide zone are moderately to pervasively altered, chlorite is the dominant secondary mineral, and O isotope values are lower (2.9–4.1‰) than elsewhere at comparable depths in the sheeted dike complex. Elsewhere in area 2, the lower dikes are moderately to pervasively altered, amphibole is the dominant secondary phase, O isotope values range from 3.6 to 5.5‰, and some localized samples show metal depletion.

3. Petrological Characteristics

3.1. Petrography

3.1.1. Volcanic sequence. The lavas are very fresh with only minor alteration to assemblages of Fe oxyhydroxides, clay minerals, and, rarely, carbonate (Table 1).

3.1.2. Sheeted dike complex. All sheeted dike samples have interacted to some degree with hydrothermal fluids (Table 1). Plagioclase is variably altered to assemblages of secondary plagioclase, chlorite, quartz, and, least commonly, epidote. In ~45% of the sheeted dike samples, plagioclase is altered to albitic plagioclase + quartz, whereas in the remaining samples quartz is absent. The albitic plagioclase and quartz assemblage is most commonly found in chlorite-rich samples from area 1 and a small zone in the central region of area 2. Clinopyroxene is partly to completely replaced by chlorite, amphibole and chlorite, or amphibole and secondary magnetite (Table 2 and Figure 2b). Secondary clinopyroxene forms as isolated blebs within, or rims on, igneous clinopyroxene in a few samples where it comprises <5% of the grain. Olivine was not identified in the sheeted dikes; however, rare clots of talc, magnetite, ± amphibole are interpreted as olivine pseudomorphs. Alteration patches include assemblages of chlorite + quartz, chlorite + amphibole, and chlorite + amphibole + quartz. Ilmenite is commonly rimmed with titanite; magnetite and sulphides are locally altered to Fe oxyhydroxides.

Veins are conspicuously rare in our sample suite. Common vein assemblages include: epidote, chlorite, and amphibole + chlorite. Where amphibole and chlorite occur together, amphibole is the earliest phase to form. Some veins and fracture surfaces have narrow (<3–5 mm) alteration halos where the groundmass is more pervasively altered than adjacent areas but to the same assemblages.

3.2. Degree of Alteration

The percent replacement of clinopyroxene by secondary phases has been determined for 97 samples (Table 2) in order to consistently document the degree of alteration in the volcanic sequence and sheeted dike complex. We selected clinopyroxene as a measure of the degree of alteration because the minerals that typically replace clinopyroxene can be reliably identified in thin section (see Table 2 for more details). Our results show that the degree of alteration in the volcanic sequence is uniformly low, whereas there is considerable regional variation in the sheeted dike complex (Figure 2b). In general, the least altered sheeted dikes come from near the volcanic–sheeted dike transition or are hosted within the gabbroic sequence whereas more pervasively altered dikes occur near the base of the sheeted dike complex (Figure 2b). Examination of the dive tracks shows that the alteration index fluctuates between adjacent samples (e.g., moderately to slightly altered) and that regional-scale changes are gradual (i.e., highly altered samples are rarely next to slightly altered samples). Discrete areas within the sheeted dike complex have either chlorite- or amphibole-dominated assemblages.

3.3. Mineral Compositions

Major element mineral compositions were determined by wavelength dispersive techniques at the University of Alberta; standard Bence-Albee corrections and natural standards were used. In the following sections, new data for the 1999 and some 1990 samples and data previously reported by *Gillis* [1995] for the 1990 samples are summarized.

3.3.1. Plagioclase. Anorthite contents (An) show a bimodal distribution with one group ranging from An_{38-70} and the other $An_{<23}$. We assume that the sodic plagiolcase group is hydrothermal as it forms patches within or rims on grains.

3.3.2. Pyroxene. Clinopyroxene has a broad range in composition ($Wo_{29-49}En_{18-52}Fs_{8-46}$; calculated assuming all iron as FeO) (Table 3; see also Figure 4 of *Gillis* [1995]). Mg # (Mg/Mg+Fe) generally ranges from 0.5 to 0.8, with a few grains having lower (down to 0.3) or higher (up to 0.85) values. Secondary clinopyroxene was identified on the basis of wollastonite component (>43–44) and the concentration of the minor elements Al_2O_3 (≤1.5 wt %), Na_2O (≤0.5 wt %), TiO_2 (≤0.5 wt %), and Cr_2O_3

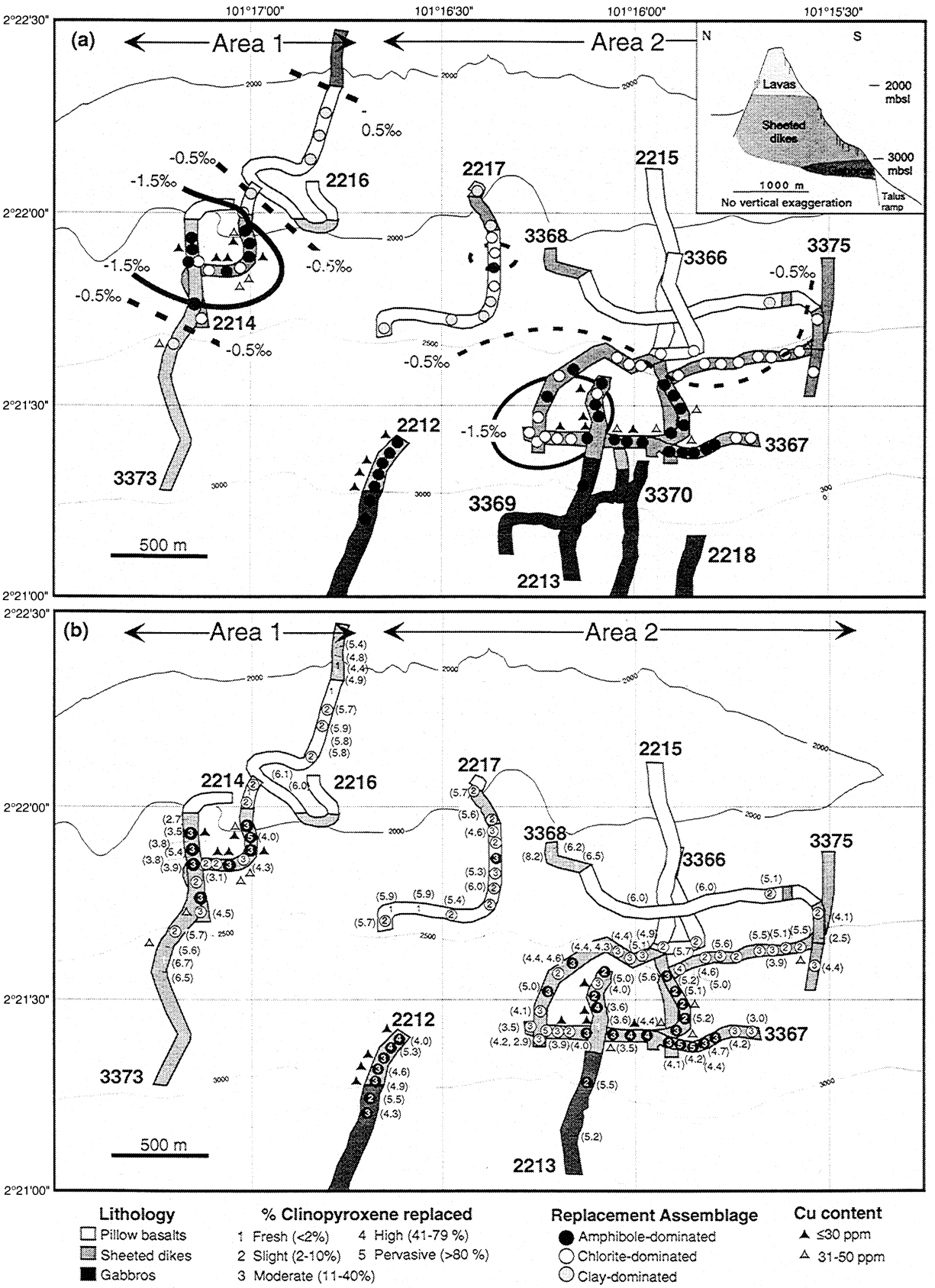
101°17'00"
101°16'30"
101°16'00"
101°15'30"
2°22'30"
2°22'00"
2°21'30"
2°21'00"
(a)
Area 1
Area 2
N
S
Lavas
2000 mbsl
Sheeted dikes
3000 mbsl
1000 m
No vertical exaggeration
Talus ramp
-0.5‰
-1.5‰
2216
2217
2215
3368
3366
3375
2214
2212
3373
3367
3369
3370
2218
2213
500 m
(b)
Area 1
Area 2
500 m
Lithology
Pillow basalts
Sheeted dikes
Gabbros
% Clinopyroxene replaced
1 Fresh (<2%)
2 Slight (2-10%)
3 Moderate (11-40%)
4 High (41-79 %)
5 Pervasive (>80 %)
Replacement Assemblage
Amphibole-dominated
Chlorite-dominated
Clay-dominated
Cu content
≤30 ppm
31-50 ppm

Table 1. Summary of Alteration Characteristics for Hess Deep and Hole 504B Crustal Rocks

	Hess Deep	Hole 504B[a]
	Primary Mineral Alteration[b]	
Volcanics		
Plagioclase	clay minerals (0–10%)	clay minerals, Fe oxyhydroxides
Clinopyroxene	clay minerals, Fe oxyhydroxides (0–10%)	clay minerals, Fe oxyhydroxides
Groundmass and void-filling phases	clay minerals, Fe oxyhydroxides; rare calcite	clay minerals, zeolites, calcite
Upper sheeted dikes		
Plagioclase	secondary plagioclase ± quartz (<20%)	albite ± prehnite ± anhydrite
Clinopyroxene	chlorite *or* amphibole ± secondary clinopyroxene (<10–40%)	chlorite ± amphibole
Groundmass and void-filling phases	chlorite, quartz, sulphides	chlorite, mixed-layer smectite/chlorite, Ca zeolites, prehnite, calcite, epidote, quartz, sulfides
Fe-Ti oxides	titanite (0-100%)	titanite
Lower sheeted dikes		
Plagioclase	secondary plagioclase ± quartz (10–100%)	albite ± calcic plagioclase ± anhydrite
Clinopyroxene	chlorite ± amphibole *or* amphibole ± secondary magnetite ± chlorite (10–100%)	amphibole ± secondary Fe-oxides
Groundmass and void-filling phases	chlorite ± quartz *or* amphibole + titanite	amphibole, chlorite, prehnite, laumontite, epidote, quartz
Fe-Ti oxides	titanite (0-100%)	titanite
	Whole rock Geochemical Fluxes[c]	
Volcanics	+ K_2O, Rb, $\delta^{18}O$ (5.7–6.7‰)	+ K_2O, Rb, $\delta^{18}O$ (5.7–13‰)
Upper sheeted dikes	– *or* nc Cu, Zn; – *or* nc $\delta^{18}O$ (2.7–5.7‰)	± CaO, Na_2O; nc Cu, Zn, S; nc *or* – $\delta^{18}O$ (4.5–6.4‰)
Lower sheeted dikes	– *or* nc Cu, Zn; – $\delta^{18}O$ (2.9–5.5‰)	± CaO, Na_2O; – K_2O; – or nc Cu, Zn, S; – $\delta^{18}O$ (3.3–5.1‰)

[a] See *Alt et al.* [1996] for references.
[b] Range in percentage replacement is given in parentheses; note that % replacement is not available for Hole 504B.
[c] Relative to fresh whole rock values; positive, addition; negative, depletion; nc, no change.

(≤0.5 wt %)[cf. *Manning and Bird*, 1986]. Hydrothermal clinopyroxene primarily occurs in the shallow sheeted dikes in area 1 and the basal dikes in area 2 (dives 2212 and 2213).

3.3.3. Amphibole. Amphiboles are dominantly calcic and fall between the actinolite–pargasite and actinolite–hornblende solid solution series (nomenclature after *Leake et al.* [1997]). A few grains of Mg-Fe-Mn amphibole were also identified. Amphibole shows typical compositional trends such that Si varies from 6.4 to 7.9 and Site A Na+K increases from 0.1 to 0.6 as Al^{iv} increases from 0.1 to 1.6 (Table 4). TiO_2 contents are generally <1 wt % although a few grains have up to 3.9 wt % (Table 4). These grains occur in the groundmass and fill vesicles and likely formed by early interaction with magmatic fluids exsolved locally during the final stages of crystallization. Mg # ranges from 0.3 to 0.8, with the most Fe-rich amphibole occurring in the coarser grained basal dikes (Figure 3). In general, amphibole Mg # are 5–15% greater than host bulk rock values, except for the coarser-grained basal dikes which show slight decreases in Mg #. Halogen contents are low (<0.3 wt %); MnO and Cr_2O_3 contents are generally low (<0.6 and <0.4 wt %, respectively). All modes of occurrence span the compositional range described above, although in a few veins, amphibole is more aluminous along vein margins than vein centers.

3.3.4. Clay minerals. Distinction between chlorite and mixed-layer smectite/chlorite was based on major element compositions such that analyses recalculated on the basis of 28 anhydrous oxygens that have Si cations <6.25 and interlayer cations (Ca+Na+K) <0.3 are considered chlorite [*Bettison and Schiffman*, 1988; *Schiffman and Fridleifsson*, 1991]. Chlorite grains contained up to 10% smectite interlayers whereas mixed-layer smectite/chlorite contained 10–55% smectite interlayers (interlayer abundance was calculated from electron microprobe data following the method outlined by *Bettison and Schiffman* [1988]). Most sheeted dike samples contain both chlorite and mixed-layer smectite/chlorite (Figure 4), which show no preferred depositional order or texture. Pure smectite primarily occurs in the volcanic sequence (e.g., dive 3368) but was also identified in a few dike samples, where it occurs as a late stage phase.

Figure 2. (a) Simplified geological and alteration map of the rift shoulder horst showing dive tracks, general lithological boundaries (based on data of *Karson et al.* [1992]; Karson et al. (unpublished cruise report, 1999); *Karson et al.* [in press]), and key alteration characteristics. The inset shows a schematic cross section of the rift shoulder horst that is oriented N–S (i.e., parallel to the strike of the dikes). Note that the 1990 dives start with "22", whereas the 1999 dives start with "33." Circles along each dive track show the location of studied samples and a general alteration index. Bold and dashed contours identify areas with similar whole rock $\delta^{18}O$ values (calculated as sample $\delta^{18}O$ values minus fresh $\delta^{18}O$ value) and highlight regional patterns. Bold contours indicate areas that are ≥1.5‰ lower than fresh values (i.e., ≤4.2‰); bold dashed contours indicate areas that are 0.5‰ lower than fresh values. (b) Detailed alteration map showing an alteration index for clinopyroxene, whole rock $\delta^{18}O$ data (per mil values in parentheses adjacent to sample location), and an index of whole rock Cu contents (symbol adjacent to a sample location indicates depletion relative to igneous values). Note that only the dive tracks along which samples included in this study were recovered are shown. Contour intervals are in meters.

Table 2. Summary of Key Alteration Characteristics for Individual Samples

Dive	Time	Lith.[a]	Clinopyroxene Alteration[b]		Whole Rock Compositions		
			% Alt.[c]	Sec. Min.[d]	Cu, ppm	Zn, ppm	$\delta^{18}O$, ‰
2212	1330	G/D	M	A	58	37	4.3
	1338	G	S	S	58	56	5.5
	1409	G	M	A	20	56	4.9
	1428	D	M	A	23	38	4.7
	1500	G/D	M	A	9	54	5.3
	1514	D	H	A	63	40	–[e]
	1524	D	H	A	13	25	4.0
2213	1125	G	M	A	70	31	5.2
	1226	G	S	A	70	34	5.5
	1351	G	F	–	17	38	3.6
	1408	G	H	A	23	34	3.6
	1439	D	S	A	53	72	–
	1504	D	M	A	40	76	4.0
	1516	G	S	A	–	–	5.0
2214	1035	D	M	C	45	100	4.5
	1036	D	M	A	55	100	–
	1040	D	S	C	58	115	–
	1130	D	M	A	9	49	3.9
	1203	D	S	C	41	104	3.1
	1214	D	S	C	29	133	–
	1240	D	M	A	13	96	–
	1257	D	S	CL	37	94	6.5
	1330	D	M	C	45	103	4.3
	1349	D	M	A	6	76	–
	1405	V	P	A	15	73	4.0
	1414	V	M	A	50	123	–
	1420	V	S	CL	54	108	6.5
	1429	V	F	CL	56	119	–
	1442	V	S	CL	55	100	6.1
2215	1041	D	M	C	52	66	3.5
	1049	D	P	C	–	–	–
	1129	D	M	C	16	52	3.9
	1157	D	S	C	–	–	–
	1214	D	M	A	59	64	4.0
	1239	D	M	A	67	88	–
	1259	D	H	A	36	70	3.5
	1328	D	H	A	52	115	4.4
	1404	D	M	A	44	118	–
	1426	D	S	A	59	93	5.2
	1453	D	S	A	46	96	–
	1515	D	S	A	70	75	5.1
2216	938	D	–	–	79	82	5.4
	946	D	–	–	66	89	4.8
	1002	D	F	–	78	80	4.4
	1017	D	F	–	54	107	4.9
	1039	D	F	–	58	94	–
	1050	V	S	CL	–	–	5.7
	1109	V	S	CL	52	105	5.9
	1144	V	–	–	65	103	–
	1156	V	–	–	–	–	5.8
	1232	V	–	–	62	104	5.8
	1255	V	–	–	77	102	–

Table 2. (continued)

Dive	Time	Lith.[a]	Clinopyroxene Alteration[b]		Whole Rock Compositions		
			% Alt.[c]	Sec. Min.[d]	Cu, ppm	Zn, ppm	$\delta^{18}O$, ‰
2216	1341	V	–	–	55	89	6.0
	1417	V	–	–	69	102	–
	1438	V	–	–	66	95	–
2217	1014	V	S	CL	–	–	5.7
	1042	V	F	–	66	117	5.9
	1054	V	F	–	58	103	5.9
	1140	V	S	CL	–	–	5.4
	1211	V	S	CL	68	113	–
	1244	V	S	CL	61	95	6.0
	1302	V	M	C	63	91	5.3
	1327	V	M	A	–	–	–
	1351	V	S	C	51	124	4.6
	1413	D	M	C	61	103	–
	1438	D	–	–	57	85	5.6
	1445	D	S	–	59	111	–
	1513	L	S	CL	61	155	5.7
	1534	?	–	–	60	147	5.1
2218	1048	G	–	–	95	25	5.7
	121O	G	–	–	23	51	3.7
	1350	D	–	–	11	57	4.2
	1404	D	P	A	54	84	3.9
	1415	D	P	A	11	106	2.9
3366	1015	D	H	C	114	85	2.9
	1021	D	–	–	80	112	4.2
	1035	D	M	C	51	77	4.1
	1058	D	M	A	65	111	5.0
	1117	D	S	C	63	102	4.4
	1124	UK/D	M	A	20	114	4.6
	1157	D	M	C	60	174	4.3
	1202	D	–	–	63	120	4.4
	1211	D	M	C	59	109	4.4
	1235	UK/D	M	C	63	105	5.1
	1257	D	S	C	50	102	4.9
	1312	D	S	C	56	110	–
3367	1107	D	P	A	47	123	4.1
	1158	D	P	A	16	84	4.2
	1239A	D	M	A	54	73	4.4
	1348	D	M	A	53	101	4.7
	1509	D	M	C	54	90	4.2
	1515	D	M	C	76	83	3.0
3368	957	D	M	C	62	113	4.4
	1117	D	–	–	75	97	2.5
	1138	D	M	C	56	90	4.1
	1251	UK	S	CL	61	92	5.1
	1305	V	–	–	48	92	6.0
	1330	V	–	–	61	96	6.0
3368	1443	UK/D	F	–	61	103	6.5
	1458	UK/D	F	–	58	87	8.2
	1506	D	–	–	47	106	6.2
3373	1147	D	F	–	97	86	6.5
	1157	UK	F	–	56	100	6.7
	1220	D	–	–	44	108	5.6

Table 2. (continued)

Dive	Time	Lith.[a]	Clinopyroxene Alteration[b]		Whole Rock Compositions		
			% Alt.[c]	Sec. Min.[d]	Cu, ppm	Zn, ppm	$\delta^{18}O$, ‰
3373	1241	D	S	CL	79	94	5.7
	1316	D	–	–	–	–	3.8
	1322	D	M	A	66	106	5.4
	1342	D	M	A	58	103	3.8
	1418	D	S	A	32	151	3.5
	1438	UK	–	–	–	–	2.7
3375	955	D	M	A	65	90	5.2
	1125	D	M	A	51	99	5.2
	1223	D	H	C	32	100	5.6
	1232	D	–	–	71	112	5.7
	1234	D	–	–	88	92	5.0
	1248	D	S	C	81	106	4.6
	1303	D	M	C	63	105	5.6
	1325	D	S	C	12	95	–
	1351	D	M	C	50	162	5.5
	1408	D	M	C	57	109	3.9
	1440	D	S	C	55	116	5.1
	1456	D	S	C	31	107	5.5

[a]Lithology: V, volcanic rock; D, sheeted dike; G, gabbro.
[b]Clinopyroxene alteration was assessed by petrographic analysis and confirmed using back scattered electron (BSE) images that were collected for 25% of the sample suite. The proportion of relict clinopyroxene and secondary minerals for 10–35 individual grains per sample was determined by analysis of the BSE images using the National Institute for Health image analysis software package. Secondary minerals were confirmed on the basis of energy dispersive X-ray spectra.
[c]Percent clinopyroxene alteration: F, fresh (<2%); S, slight (2–10%); M, moderate (11–40%); H, high (41–80%); and P, pervasive (81–100%).
[d]Sec. Min., secondary mineral replacing clinopyroxene: A, amphibole; C, chlorite; CL, clay minerals.
[e]No data.

Chlorite and mixed-layer smectite/chlorite compositions are given in Table 5 and are dominantly clinoclore with minor chamosite (classification after *Bailey* [1988]). Mg # range from 0.4 to 0.7 (Figure 4) and are typically 5–15% higher than host bulk rock values; the greatest shift occurs in area 1. Chlorites from area 1 have the same Mg # (0.6–0.7) as primary chlorite from hydrothermal breccias recovered from area 1 (dive 2214) [*Saccocia and Gillis*, 1995] which suggests that Mg # are at least locally controlled by fluid compositions. FeO^T contents vary regionally such that the lowest values occur in area 1 and FeO^T increases with depth (Figure 4). MnO contents are generally ≤0.30 wt % with a few grains up to 0.6 wt %. Cl and F contents are below detection limits. Chlorite and mixed-layer smectite/chlorite show no variation in composition with the degree of replacement of clinopyroxene or their presence in chlorite- versus amphibole-dominated samples.

3.3.5. Epidote. Epidote is not a common mineral in the Hess Deep sheeted dikes and locally replaces plagioclase and interstitial zones and fills veins. $Fe^{3+}/(^{vi}Al+Fe^{3+})$ ratios range from 0.22 to 0.34 and are similar to epidote in the hydrothermal breccias from area 1 [*Saccocia and Gillis*, 1995].

4. Bulk Rock Compositional Changes

4.1. Major and Trace Element Compositions

Assessment of major and trace element mobility is complicated at Hess Deep by the remarkable range in primary MOR basalt (MORB) chemistry within the volcanics and sheeted dikes [*Stewart*, 2000]. Hence we limit our discussion to the mobile elements that provide some insight into the conditions of alteration. K_2O and Rb are variably enriched in the volcanic sequence and zones of mixed volcanics and dikes (Figure 5). In area 1, alkali enrichment is greatest in the lava sequence but also shows enrichment near the base of dive 3373 where a mixed zone of volcanics and dikes underlies shallower exposures of massive sheeted dikes. In area 2, samples from deeper in the volcanic sequence where the lavas are highly fractured show slightly greater enrichment than those from shallower depths, presumably due to enhanced permeability. The sheeted dike complex is uniformly depleted in K_2O and Rb throughout the field area (Figure 5). Alkali depletion is an axial processes that results from fluid-rock exchange at high temperatures (>200°C) whereas alkali uptake by secondary clay minerals occurs at low temperatures and is primarily an off-axis phenomenon [*Thompson*, 1983]. It is interesting to note that dikes which intrude high into the volcanic sequence (e.g., dives 2217 and 3368) are also depleted in alkalis, whereas associated lavas (collected within a few tens or hundreds of meters) either have igneous values or are enriched. This suggests that the alkali elements were mobilized during short-lived, very localized hydrothermal events.

Cu and Zn retain igneous values in the volcanic sequence and are variably depleted in the sheeted dike complex (Figure 5). Cu shows preferential mobilization over Zn due to the relative stability of the hosts of these elements (e.g., sulphides versus Fe-Ti oxides). Metal depletion is most pronounced in the shallow sheeted dikes in area 1, where several samples show >50% de-

Table 3. Representative Clinopyroxene Compositions[a]

	Sample				
	2214-1240	2214-1240	2213-1408	3367-1509	3368-1138
Area	1	1	2	2	2
Alt. type[b]	A-3	A-3	A-4	C-3	C-3
Occurence[c]	H	M	H	H	M
SiO_2	53.24	51.17	52.81	52.23	49.54
TiO_2	0.10	0.59	0.21	0.13	1.43
Al_2O_3	0.71	2.02	1.16	0.58	2.56
FeO^T	11.20	15.53	4.89	12.60	16.23
Cr_2O_3	0.08	0.00	0.23	0.00	0.02
MnO	0.70	0.43	0.19	0.51	0.38
MgO	11.60	12.19	15.90	11.06	12.28
CaO	22.92	18.24	24.64	22.02	17.69
Na_2O	0.18	0.25	0.17	0.13	0.32
Total	100.71	100.41	100.20	99.257	100.45
Cation Proportions on the Basis of 6 Oxygens					
Si	2.00	1.94	1.93	2.00	1.88
Al	0.03	0.09	0.05	0.03	0.11
Ti	–	0.02	0.01	–	0.04
Fe	0.35	0.49	0.15	0.40	0.52
Cr	–	–	–	–	–
Mg	0.65	0.69	0.87	0.63	0.70
Mn	0.02	0.01	0.01	0.02	0.01
Ca	0.92	0.74	0.97	0.90	0.72
Na	0.01	0.02	0.01	0.01	0.02
Wo	0.47	0.38	0.49	0.46	0.37
En	0.33	0.36	0.44	0.32	0.36
Fs	0.19	0.26	0.08	0.21	0.27
Mg #	0.65	0.58	0.85	0.61	0.57

[a]In wt %; Wo, wollastonite; En, enstatite; Fs, ferrosalite.
[b]Alteration types: A, amphibole-dominated; C, chlorite-dominated; CL, clay-dominated; 1, fresh (<2%); 3, moderate (11–40%); 4, high (41–80%).
[c]Occurrence: H, hydrothermal; M, magmatic.

pletion, and in the basal dikes of area 2 recovered along dives 2212 (Figure 2b). Other metal-depleted samples are sporadically distributed throughout the area. The range in MnO can generally be explained by igneous processes (e.g., covaries with FeO_T); the few samples that show MnO enrichment are sporadically distributed throughout the field area (Figure 5).

4.2. Whole Rock O Isotope Data

Ninety-seven whole rock samples were analyzed for $\delta^{18}O$ at the University of Alberta (Table 2). Whole rock powders were reacted with BrF_5 at 625°C to liberate oxygen [*Clayton and Mayeda*, 1963]. Oxygen was converted to CO_2 and analyzed for its isotopic ratio on a Finnigan-MAT 252 mass spectrometer. The data are reported in the usual delta notation with respect to the SMOW standard [*Craig*, 1961] using a water/CO_2 fractionation factor of 1.0407 to insure compatibility of these data with previous studies of mid-ocean ridge rocks. On this scale, NBS-28 quartz has a value of 9.35‰. Analytical reproducibility was ±0.1‰.

The O isotope data range widely from 2.5 to 8.2‰, when compared to the unaltered crust (5.7 ± 0.3‰) and show a bimodal distribution with peaks at 4.25 and 5.5‰ (Figure 6). The $\delta^{18}O$ values for our *Alvin* samples are indistinguishable from whole rock O isotope data for other Hess Deep samples recovered during the French *Nautile* dive program [*Agrinier et al.*, 1995] and the ODP Leg 147 drill core [*Lécuyer and Gruau*, 1996].

The high density of sampling by the submersible permits the interpretation of the oxygen isotope data in terms of field relations. The highest $\delta^{18}O$ values come from the volcanics where $\delta^{18}O$ enrichment reflects incipient weathering by ambient seawater. In comparison to other MORB suites the Hess Deep volcanics are only slightly $\delta^{18}O$ enriched as would be expected from their young age [*Manac'h et al.*, 1999; *Muehlenbachs and Clayton*, 1972]. The sheeted dikes and gabbros have lower $\delta^{18}O$ values as a result of interaction with high temperature hydrothermal fluids. Contouring of the sheeted dike $\delta^{18}O$ data (Figure 2a) reveals two low-$\delta^{18}O$ centers (≥400-m-wide) located near the sheeted dike–volcanic transition in area 1 and the sheeted dike–gabbro transition in area 2. In area 1 the transition from the low-$\delta^{18}O$ center into the surrounding, less depleted areas occurs over a narrow interval (<200 m). To the south, this abrupt change is due a change in lithology to a mixed zone of dikes and volcanics. To the north and east, it reflects a rapid change in lithology, from sheeted dikes to volcanics. In area 2 the low $\delta^{18}O$ center grades gradually into less depleted areas within the sheeted dike complex.

Interpretation of these regional O isotope patterns (Figure 2) is not straightforward because whole rock $\delta^{18}O$ values reflect the combined effects of temperature, modal mineralogy, and fluid composition [e.g., *Elthon et al.*, 1984; *Muehlenbachs and Clayton*, 1972; *Stakes and O'Neil*, 1982]. We use a modified version of the closed system oxygen isotope exchange model of *Taylor*

Table 4. Representative Amphibole Compositions[a]

	Sample							
	2214-1036	2214-1240	2215-1041	2217-1327	2212-1527	3375-1456	3367-1509	3367-1158
Area	1	1	2	2	2	2	2	2
Alt. type[b]	A-3	A-3	C-3	A-3	A-4	C-2	C-3	A-5
Occurrence[c]	vein	cpx rep	vein	vein	cpx rep	vesicle	cpx rep	plag rep
SiO_2	52.35	46.94	49.45	52.60	46.79	46.15	50.33	51.51
TiO_2	0.52	0.16	0.48	0.23	0.94	3.93	0.39	0.30
Al_2O_3	3.15	7.10	5.20	1.87	7.26	6.12	4.71	3.38
FeO^T	18.13	22.32	20.26	20.73	17.89	16.13	16.78	17.36
Cr_2O_3	0.04	0.02	0.40	0.50	0.03	0.00	0.09	0.00
MnO	0.24	0.43	0.07	0.03	0.23	0.61	0.31	0.42
MgO	13.45	11.12	12.09	10.72	14.51	14.35	12.43	12.46
CaO	10.51	10.06	9.64	11.44	8.76	9.49	12.11	11.95
Na_2O	0.56	0.23	1.10	0.31	0.80	1.40	0.36	0.29
K_2O	0.06	0.04	0.03	0.08	0.17	0.34	0.05	0.06
F	0.00	0.00	0.22	0.00	0.00	0.50	0.00	0.00
Cl	0.19	0.00	0.00	0.00	0.18	0.25	0.02	0.06
Total	99.20	98.41	98.92	98.51	97.56	98.99	97.57	97.78
	Cation Proportions on the Basis of 23 Anhydrous Oxygens							
Si	7.61	6.92	7.30	7.81	6.86	6.80	7.37	7.58
Al^{iv}	0.39	1.09	0.70	0.19	1.14	1.06	0.63	0.42
Al^{vi}	0.15	0.15	0.21	0.14	0.12	0.00	0.19	0.16
Ti	0.06	0.02	0.05	0.03	0.10	0.44	0.04	0.03
Cr	0.01	0.00	0.05	0.06	0.00	0.00	0.01	0.00
Mg	2.92	2.44	2.66	2.37	3.17	3.15	2.71	2.73
Fe^{2+}	2.21	1.92	2.48	2.58	1.65	1.97	1.71	2.04
Fe^{3+}	0.00	0.83	0.02	0.00	0.55	0.02	0.34	0.10
Mn	0.03	0.05	0.01	0.00	0.03	0.08	0.04	0.05
Ca	1.64	1.59	1.53	1.82	1.38	1.50	1.90	1.88
K	0.01	0.01	0.01	0.02	0.03	0.06	0.01	0.01
Na	0.16	0.07	0.31	0.09	0.23	0.40	0.10	0.08
Sum A (Na+K)	0.17	0.07	0.32	0.10	0.26	0.16	0.06	0.09
Total cations	15.17	15.07	15.32	15.10	15.26	15.46	15.06	15.09
Mg #	0.57	0.56	0.52	0.48	0.66	0.62	0.61	0.57

[a]In wt %; recalculated on the basis of 23 anhydrous oxygens following the normalization of *Robinson et al.* [1982]; structural formulae were averaged for analyses whose charge balance was satisfied by both the 13 CNK and 15 NK normalization schemes.

[b]Alteration type; A, amphibole-dominated; C, chlorite-dominated; CL, clay-dominated; 1, fresh (<2%); 3, moderate (11–40%); 4, high (41–80%).

[c]Occurrence; cpx rep, clinopyroxene replacement; plag rep, plagioclase replacement.

[1977], which accounts for the modal mineralogy of altered rocks [*Elthon et al.*, 1984], to evaluate the effects of isotopic exchange at various temperatures for chlorite- and amphibole-rich rocks (Figure 7). We acknowledge that these simple calculations do not account for the specific details of reaction progress [e.g., *Bowers and Taylor*, 1985; *Shanks et al.*, 1995] and that closed systems are not indicative of natural conditions. However, the isotopic equilibrium curves provide reasonable estimates of relative water/rock ratios prevalent in different regions of our field area during alteration. Our model assumes that the sheeted dikes were completely altered to either chlorite- or amphibole-dominated assemblages (Figure 7; see caption for model details). Comparison of our whole rock data with the equilibrium curves, in conjunction with temperature constraints (see section 5), shows that alteration assemblages from different areas have distinctive $\delta^{18}O$–water/rock ratio relationships. The highest water/rock ratios in our field area are found within the low-$\delta^{18}O$ centers in areas 1 and 2, with chlorite-rich samples showing lower values than amphibole-rich samples (Figure 7). By contrast, amphibole-rich rocks from the basal sheeted dikes east and west of the low-$\delta^{18}O$ center were altered at the lowest water/rock ratios. Similarly low water/rock ratios have also been estimated for gabbroic rocks from the Hess Deep area on the basis of $\delta^{18}O$ data for mineral pairs [*Agrinier et al.*, 1995] and an O isotopic diffusion model for plagioclase [*Lécuyer and Reynard*, 1996]. This suggests that the permeability within amphibole-dominated basal sheeted dikes was not significantly different from that in the subjacent gabbroic sequence during high-temperature alteration.

5. Temperature Estimates

5.1. Pyroxene

Minimum temperatures of formation for hydrothermal clinopyroxene, estimated using the 1-atm pyroxene experiments of *Lindsey* [1983], range from 500 to 750°C and place the magmatic to hydrothermal transition at 700–750°C [this study; *Gillis*,

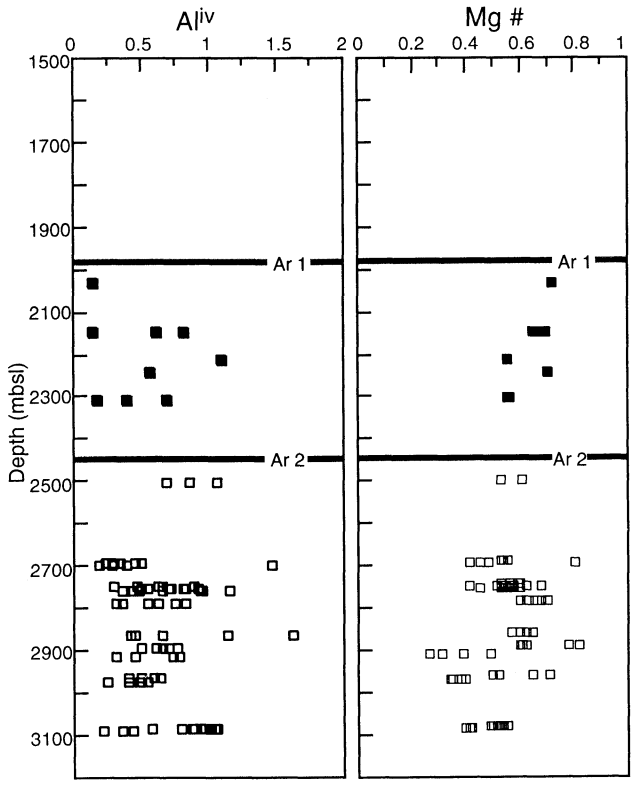

Figure 3. Amphibole compositions (Al^{iv}, Mg #) versus depth sorted by geographical area. The average depth of the volcanic–sheeted dike transition (indicated by shaded horizontal line) occurs at different depths in areas 1 and 2. Individual samples are not differentiated by lithology as the fractured nature of the outcrop made the distinction between dike or volcanic subjective in many cases. Solid squares are for samples from area 1; open squares are for samples from area 2. Recalculated on the basis of 23 anhydrous oxygens following the normalization of *Robinson et al.* [1982]; structural formulae were averaged for analyses whose charge balance was satisfied by both the 13 CNK and 15 NK normalization schemes.

1995]. See *Gillis* [1995] for a discussion of the limitations of these estimates.

5.2. Plagioclase–Amphibole

Equilibrium temperatures were calculated for plagioclase–amphibole pairs from seven sheeted dike samples (Table 6) using the exchange thermometers developed by *Holland and Blundy* [1994]. These thermometers are appropriate for silica-saturated or undersaturated rocks in the range of 400–900°C, with an uncertainty of ±40°C. Igneous plagioclase adjacent to amphibole is replaced by a narrow rim (5 to >20 μm) of secondary plagioclase whose anorthite content is typically shifted toward lower values. The compositional homogeneity of these rims and rapid reaction rates at amphibolite facies conditions [*Wood and Walther*, 1983] indicate that equilibrium was achieved on a local scale [cf. *Manning et al.*, 1996]. Calculated temperatures for five samples from the basal dikes from area 2 ranged from 609 to 733°C, with an average of 658°C (n=22). Similar high temperatures were calculated for one dike sample (dive 2214) from area 1 and one high-level dike sample (dive 2217) hosted in the volcanic sequence in area 2. An attempt was made to apply this thermometer for several other dike samples, but it was not possible to find appropriate equilibrium pairs. It is notable that these temperatures are only slightly lower than average peak temperatures (≥700°C) recorded in the gabbroic sequence [*Manning et al.*, 1996; *Weston*, 1998; K. Gillis, unpublished data, 2000].

5.3. Chlorite

A variety of empirically and thermodynamically based geothermometers have been proposed for chlorite, although none have been shown to be broadly applicable [*de Caritat et al.*, 1993]. *Cathelineau and Nieva* [1985] and *Cathelineau* [1988] reported that Al^{iv} systematically increased with increasing temperature in altered andesites from the Los Azufres geothermal system. Their empirical thermometer has been successfully applied to chlorite and mixed-layer smectite/chlorite from some other geothermal systems [*Cathelineau and Nieva*, 1985] and regionally metamorphosed metabasaltic terrains [*Bevins et al.*, 1991].

We have applied the *Cathelineau* [1988] thermometer to our chlorite data in order to evaluate if there are regional variations in formation temperature. Chlorite and mixed-layer smectite/chlorite compositions were recalculated on the basis of 14 anhydrous O and excluded the interlayer cations Ca, K, and Na [*Cathelineau and Nieva*, 1985]; the cumulative error of the thermometer is ~50°C [*Laverne et al.*, 1995]. Calculated temperatures range from 60 to 345°C (Figure 4). Within the shallow dikes, maximum temperatures in area 1 (~316°C) are higher than those in area 2 (~250°C). Within area 2, temperatures increase from ~250°C in the shallow sheeted dikes to ≤345°C in the basal dikes (Figure 4). Our data show that temperatures decrease as the smectite component of chlorite and mixed-layer smectite/chlorite increases, consistent with other studies [e.g., *Bevins et al.*, 1991; *Laverne et al.*, 1995]. Although it may be interpreted that chlorite was progressively overprinted by mixed-layer smectite/chlorite as temperatures decreased, other parameters related to reaction progress (e.g., reaction kinetics, water/rock ratio, time) could also contribute to the coexistence of chlorite and mixed-layer smectite/chlorite [e.g., *Velde et al.*, 1991].

5.4. Mineral Assemblages

The sheeted dikes are altered to greenschist and amphibolite facies mineral assemblages. On the basis of experimental studies [e.g., *Liou et al.*, 1974; *Moody et al.*, 1983], samples that contain amphibole and lack chlorite formed at temperatures >450°C, whereas samples that contain both amphibole and chlorite likely equilibrated at lower temperatures (250-450°C). See *Gillis* [1995] for discussion of these constraints.

6. Comparison With ODP Hole 504B

Most of our knowledge about alteration processes in modern oceanic volcanic sequences and, in particular, sheeted dike complexes comes from extensive study of the Deep Sea Drilling Project (DSDP)/ODP Hole 504B drill core (see *Alt et al.* [1996] for synthesis). Although recovery diminished significantly downhole (~11% in the lower dikes), these cores, in combination with extensive downhole logging, have provided the "geological ground truth" for many aspects of our current models for oceanic hydrothermal systems, both on and away from the spreading axis. Detailed comparison between Hole 504B and Hess Deep (Table 1) provides a test of the representativeness of Hole 504B and should reveal the influence of crustal age and spreading rate on alteration

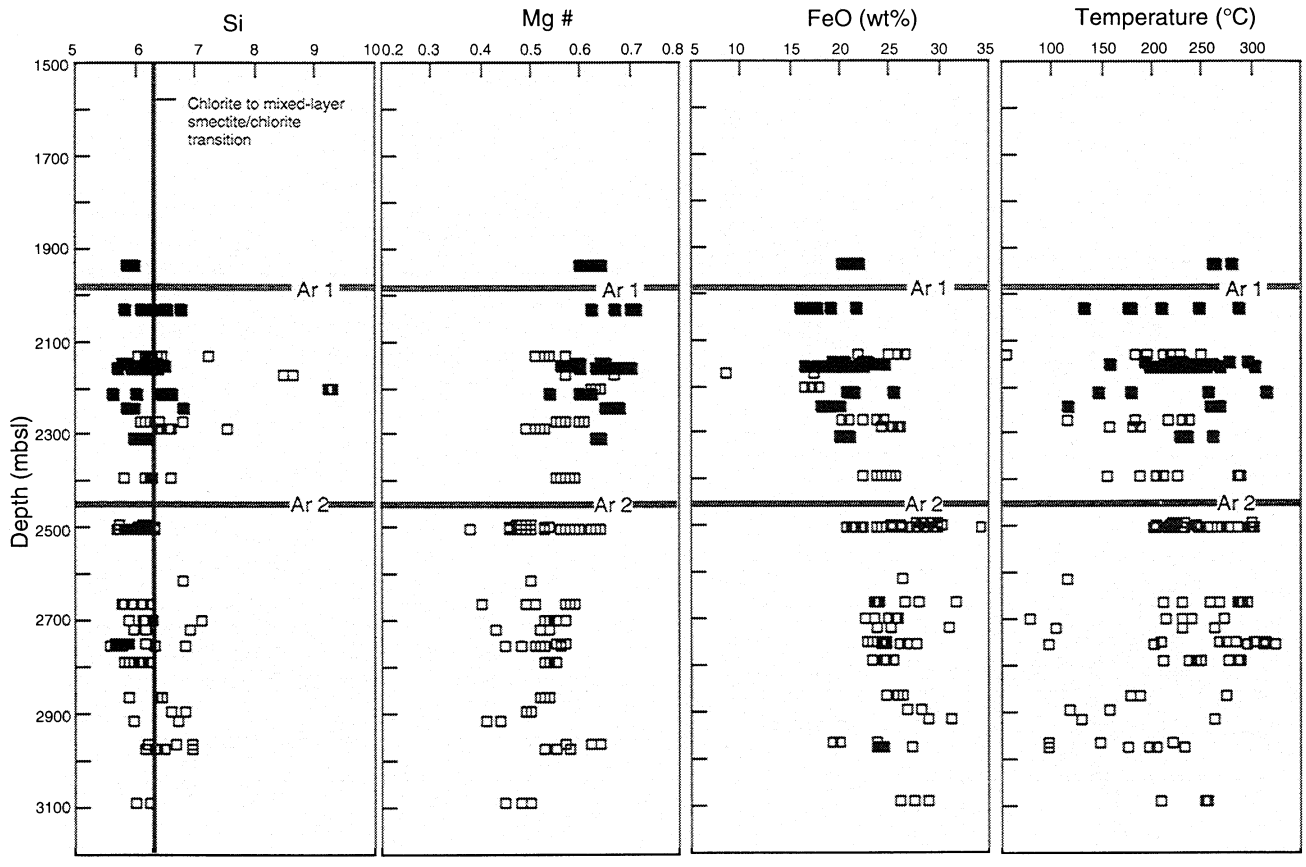

Figure 4. Chlorite compositions (Si, Mg #, FeO^T) versus depth sorted by geographical area. Temperatures calculated using the *Cathelineau* [1988] thermometer are also shown. Symbols are the same as in Figure 3.

patterns as Hole 504B sampled older crust (5.9 Ma) than Hess Deep (1.2 Ma) and formed at an intermediate spreading ridge.

Alteration characteristics of the Hole 504B and Hess Deep volcanic sequences are generally similar; however, the degree of alteration is significantly less at Hess Deep. Whole rock compositions show a similar enrichment in K_2O [*Alt et al.*, 1986b] whereas O isotope values are generally lower at Hess Deep than Hole 504B [*Alt et al.*, 1986a]. Late-stage carbonates and zeolites are very rare at Hess Deep but are common phases in Hole 504B [*Alt et al.*, 1986a]. These differences suggest that the alkali element uptake by low temperature phases (i.e., clay minerals) occurs very early (≤1 Myr), whereas O isotopic exchange continues for several millions years [*Muehlenbachs*, 1986]. Moreover, carbonate and zeolite formation occurs within a 1 to >5 Myr time frame, as predicted by *Staudigel et al.* [1981].

Many of the petrological and geochemical characteristics documented for Hess Deep have been observed in the sheeted dike section of Hole 504B (Table 1). Here we highlight a few notable differences. In Hole 504B, chlorite only replaces clinopyroxene in the shallow sheeted dikes [*Ishizuka*, 1989], whereas this relationship is prevalent throughout the Hess Deep sheeted dike complex. Similarly, metal (Cu, Zn) and O isotope (<4.5‰) depletion at Hole 504B is restricted to the lower dikes [*Alt et al.*, 1996], whereas these elements are locally depleted at different depths and localities along the scarp. The depth-related trends in the Hole 504B dikes are most similar to Hess Deep dikes from the eastern half of area 2 (Figures 2 and 5). Differences between Hole 504B and the Hess Deep dikes exposed elsewhere in the field area likely reflect regional-scale fluid flow patterns (see section 7). We find no reason to attribute these differences to the spreading environment (i.e., fast versus intermediate spreading rates). Similar to the volcanic sequence, the sheeted dike complex at Hess Deep lacks the late stage veins of Ca zeolites, prehnite and calcite that are prevalent in Hole 504B due to its young age.

7. Discussion

The alteration patterns documented for this 4-km-wide region within the sheeted dike complex represent ~60,000 years of spreading history, assuming the current spreading rate of 130 mm/yr. It is likely that these exposures formed at the same ridge segment and probably near the same area along that segment (e.g., segment center versus distal end). While we acknowledge that the exposures at Hess Deep may represent an amalgamation of crustal blocks with disparate spreading origins [e.g., *Lonsdale*, 1999], we have found no evidence that the narrow window of crustal exposures examined here is composed of more than one crustal block. Hence the spatial variability in alteration characteristics documented for Hess Deep provides a temporal record of evolving physical and chemical conditions for a fast spreading ridge segment. We start by discussing the evolution of hydrothermal alteration in the oldest part of the field area (area 2) and move west into slightly younger crust (area 1).

7.1. Area 2: Recharge, Reaction Zones?

In area 2 the transition from lavas to sheeted dikes occurs over a few tens to hundreds of meters, the sheeted dikes are locally highly fractured and have been rotated to the east, and the gab-

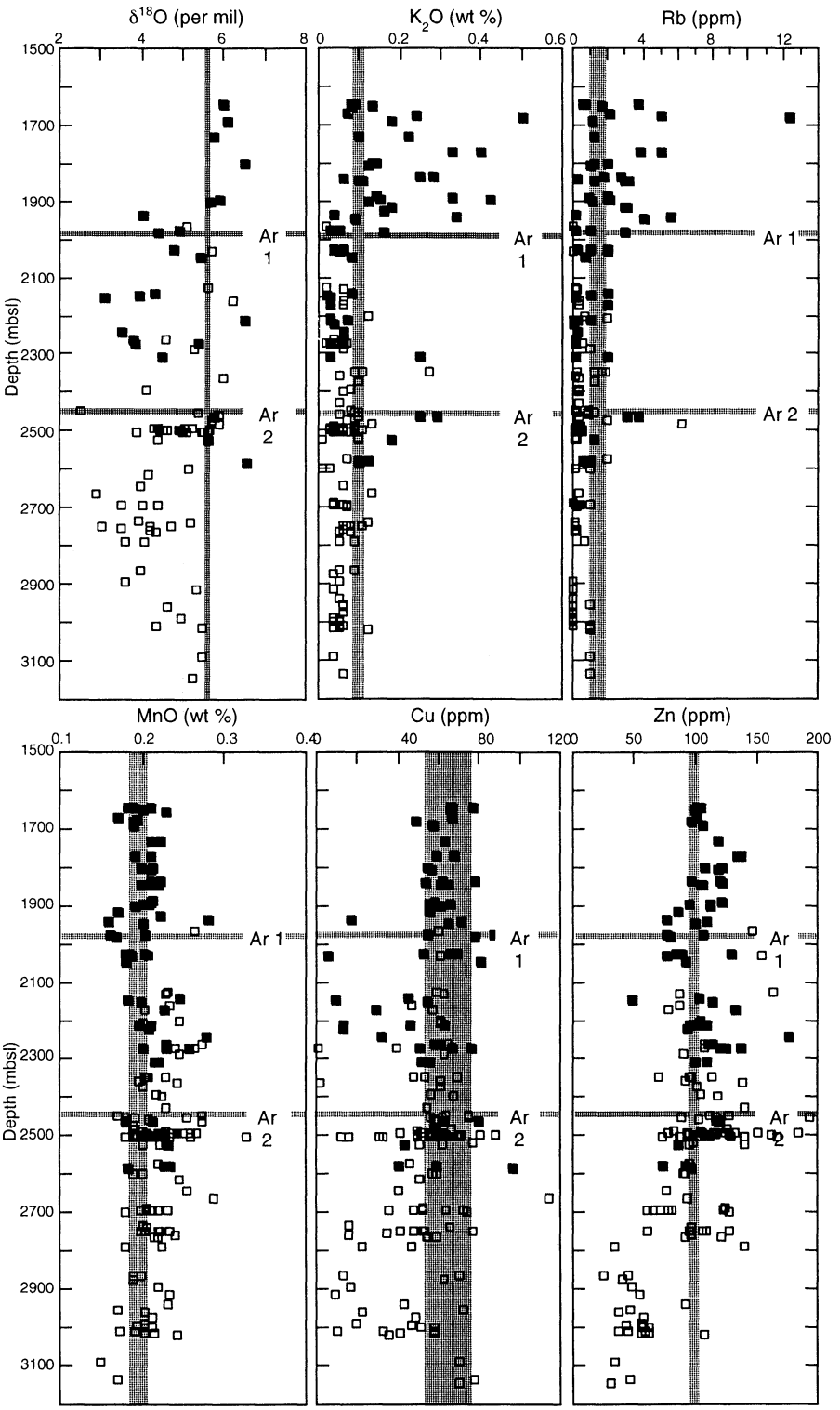

Figure 5. Bulk rock compositions ($\delta^{18}O$, K_2O, Rb, MnO, Cu, Zn) versus depth. Average fresh rock values (±1 standard deviation) are shown as vertical bars for reference (data sources are $\delta^{18}O$ from *Taylor* [1968] and *Muehlenbachs and Clayton* [1972]; K_2O, Rb, Cu, Zn, MnO 9°N EPR data from RIDGE Petrological database of the ocean floor available at http://www.EarthRef.org/GERM/bottom.htm). Major and trace element compositions of the 1999 and 1990 samples were analyzed by direct current plasma spectroscopy (K_2O, MnO, Zn) and inductively coupled mass spectrometry (Rb, Cu) at Duke University [*Stewart*, 2000]. Cu values shown for a subset of the 1990 samples were analyzed by X-ray fluorescence at the Woods Hole Oceanographic Institution [J. Natland, unpublished data, 1992]. Comparison of Cu data for samples analyzed by both methods shows <5% variation. Symbols are the same as in Figure 3.

Table 5. Representative Chlorite and Mixed-Layer Smectite/Chlorite Compositions[a]

	Sample									
	2214-1036	2214-1240	2214-1240	3373-1418	2215-1041	3366-1035	3366-1157	3367-1509	3368-1443	3375-1223
Area	1	1	1	1	2	2	2	2	2	2
Alt. type[b]	A-3	A-3	A-3	A-3	C-3	C-3	C-3	A-3	CL-1	A-4
Occurrence[c]	vein	gm	gm	cpx rep	vein	cpx rep	plag rep		vesicle	gm
SiO_2	30.13	26.39	32.35	30.29	26.59	28.67	29.16	26.76	46.24	28.63
TiO_2	0.04	0.05	0.05	0.07	0.00	0.13	0.04	0.05	0.06	0.01
Al_2O_3	16.36	18.24	14.22	18.36	18.26	17.10	15.10	18.66	4.05	16.85
FeO^T	20.92	25.30	21.52	19.98	27.38	28.03	29.14	24.68	16.53	28.81
Cr_2O_3	nd	nd	nd	0.00	nd	0.03	0.02	0.28	0.00	0.00
MnO	0.26	0.29	0.00	0.25	0.52	0.18	0.27	0.30	0.03	0.40
MgO	19.59	16.34	18.26	20.92	15.27	14.97	15.25	16.60	16.56	13.83
CaO	0.45	0.09	1.56	0.23	0.02	0.51	0.12	0.04	0.20	0.29
Na_2O	nd	nd	nd	0.05	nd	0.06	0.10	0.02	0.33	0.03
K_2O	nd	nd	nd	0.12	nd	0.02	0.10	0.01	0.54	0.31
Total	87.75	86.70	87.95	90.27	88.04	89.72	89.33	87.41	84.56	89.18
	Cation Proportions on the Basis of 28 Anhydrous Oxygens									
Si	6.17	5.64	6.62	5.99	5.66	5.98	6.15	5.66	9.31	6.04
A^{iv}	1.83	2.36	1.38	2.01	2.34	2.02	1.85	2.34	0.00	1.96
Al^{vi}	2.12	2.23	2.05	2.26	2.23	2.18	1.91	2.31	0.96	2.23
Ti	0.01	0.01	0.01	0.01	0.00	0.02	0.01	0.01	0.01	0.00
Fe	3.59	4.52	3.68	3.30	4.87	4.89	5.14	4.37	2.78	5.09
Mn	0.05	0.05	0.00	0.04	0.09	0.03	0.05	0.05	0.01	0.07
Mg	5.98	5.21	5.57	6.17	4.84	4.65	4.80	5.24	4.97	4.35
Ca	0.10	0.02	0.34	0.05	0.01	0.11	0.03	0.01	0.04	0.07
Na	0.00	0.00	0.00	0.02	0.00	0.02	0.04	0.01	0.13	0.01
K	0.00	0.00	0.00	0.03	0.00	0.01	0.03	0.00	0.14	0.08
Total cations	19.84	20.05	19.65	19.88	20.05	19.91	19.99	20.00	18.34	19.90
(Ca+K+Na)	0.10	0.02	0.34	0.10	0.01	0.14	0.10	0.02	0.31	0.16
Percent chlorite[d]	0.96	1.00	0.88	0.96	1.01	0.96	0.98	1.00	0.45	0.96
Temperature (°C)[e]	228	316	146	258	314	258	232	313	–	248

[a]In wt %; nd, not determined.
[b]Alteration type: A, amphibole-dominated; C, chlorite-dominated; CL, clay-dominated; 1, fresh (<2%); 3, moderate (11–40%); 4, high (41–80%).
[c]Occurrence: gm, groundmass; cpx rep, clinopyroxene replacement; plag rep, plagioclase replacement.
[d]Calculated following method outlined by *Bettison and Schiffman* [1988].
[e]Temperature calculated using the geothermometer of *Cathelineau* [1988].

bro–sheeted dike transition is marked by a narrow zone of intercalated dikes and gabbros. Along the eastern (dives 3367 and 3375; eastern half of dives 2215, 3366) and western (dives 2212, 2217) margins of area 2, a typical "drill core" trend is observed in the sheeted dike complex (Figure 8a). With increasing depth the dominant secondary mineral changed from chlorite to amphibole, and the degree of recrystallization and calculated temperatures (≤250 to >550°C) increased. Whole rock $\delta^{18}O$ values decrease from 4.4 to 5.5‰ in the upper dikes to 3.5 to 4.5‰ within the basal dikes and are indicative of low water/rock ratios (Figure 7).

The basal sheeted dikes that occur within a few hundred meters of the gabbroic sequence (e.g., dive 3367) exhibit some variability in alteration on a scale of tens to hundreds of meters. Calculated temperatures for a few samples are very high (631–756°C), whereas mineral assemblages for other samples indicate lower temperatures (≤450°C). These basal dikes also show localized metal mobility (Figure 2b) and a range in $\delta^{18}O$ values (Figure 2). These small-scale variations record transient changes in temperature and permeability that may be explained by magmatic processes. Theoretical models predict that the basal sheeted dike complex is a dynamic region where there are significant fluctuations in temperature and permeability [*Wilcock and Delaney*, 1996]. When a dike intrudes into the sheeted dike complex, it creates permeability adjacent to its margins, but these fractures are subsequently sealed due to thermal elastic stresses and hydrothermal mineral precipitation [*Curewitz and Karson*, 1998; *Lowell et al.*, 1993]. Dike injection also causes a short-lived perturbation in the steady state thermal structure imposed from below by a melt lens [*Wilcock and Delaney*, 1996]. Although we cannot explicitly test these predictions with our field data, the alteration characteristics in the basal sheeted dikes are consistent with fluctuations in temperature and water/rock ratios. Many features of this area (e.g., stratigraphic position, low water/rock ratios) make it compelling to propose that a hydrothermal "reaction zone" was centered in this section of basal dikes at the ridge axis. If this were the case, it may be expected that the basal dikes would be more uniformly metal-depleted than they are. Hence the alteration characteristics of these basal dikes do not require formation within a "reaction zone."

The central region of area 2 (intersection of dives 3366 and 2215, SW end of tracks) shows yet another style of alteration (Figure 8b). A low-$\delta^{18}O$ center is located near the sheeted

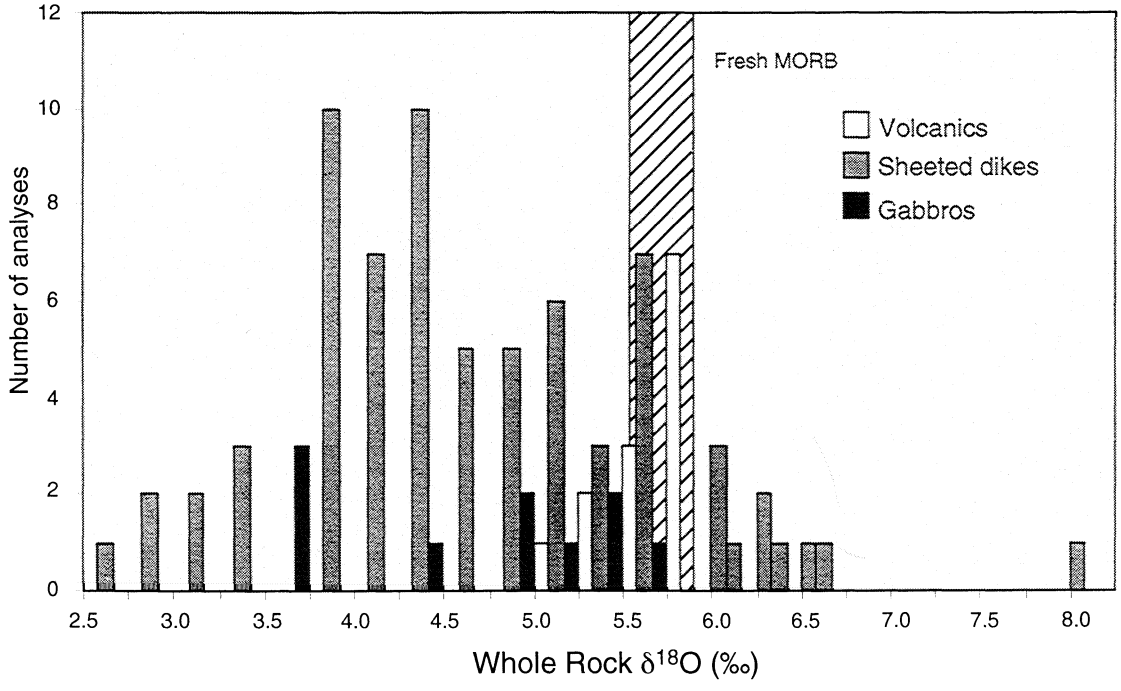

Figure 6. Histogram of whole rock O isotope data sorted by lithology. The range of fresh MORB values shown for comparison is from *Muehlenbachs and Clayton* [1972].

dike–plutonic transition (Figure 2) where outcrops are composed of highly fractured sheeted dikes. In general, as chlorite-dominated assemblages grade outward into amphibole-dominated assemblages, there is a concomitant increase in $\delta^{18}O$ values. In contrast to the basal dikes to the east and west, there is no evidence for very high temperature alteration (>450°C), but metal mobilization shows similar local variability. The $\delta^{18}O$ values reflect the modal abundance of chlorite that in turn is indicative of higher water/rock ratios than elsewhere (Figure 7). It is likely that fluids became focused in this area during a period of enhanced tectonic activity at the spreading axis, although the direction of flow cannot be determined. Alternatively, if the fracturing and

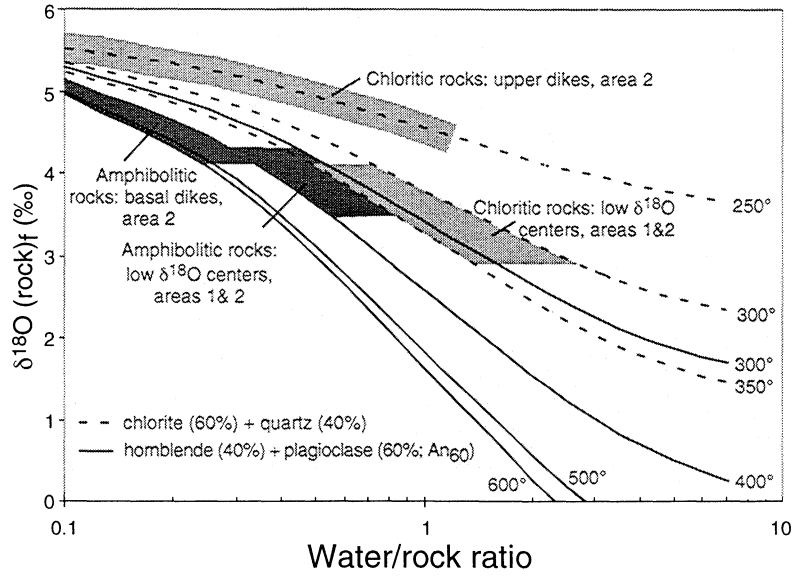

Figure 7. Modeling of final $\delta^{18}O$ rock values versus water/rock ratio for samples altered to chlorite- and amphibole-dominated assemblages at various temperatures. Curves are for closed system interaction using the equation of *Taylor* [1977], where initial rock $\delta^{18}O$ = 5.7‰ [*Taylor*, 1968; *Muehlenbachs and Clayton*, 1972; *Ito and Clayton*, 1982]; initial fluid $\delta^{18}O$ = 0‰ [*Epstein and Mayeda*, 1953]; and final fluid $\delta^{18}O$ = 1‰ (midpoint of EPR vent fluids [*Shanks et al.*, 1995]). Temperature-dependent mineral water oxygen isotope fractionations used are chlorite [*Cole and Ripley*, 1998]; quartz [*Matsuhisa et al.*, 1979]; hornblende [*Zheng*, 1993]; and plagioclase [*O'Neil and Taylor*, 1967]. Reported water/rock ratios are defined by atom percent oxygen in different phases [*Stakes and O'Neil*, 1982].

Table 6. Summary of Thermometric Calculations[a]

Sample	Area	Amphibole-Plagioclase[a]			Chlorite[c]	
		Range	Average ± SD.	N[d]	Range	N[d]
2213-1408	2	747–773	757 ± 11	4	no chlorite	–
2214-1240	1	613–681	649 ± 31	4	146–316	4
2215-1328	2	609–739	655 ± 62	7	no chlorite	–
2215-1041	2	662	–	1	202–324	6
2217-1327	2	672–717	683 ± 17	5	184–238	5
3367-1158	2	588–651	609 ± 36	6	no chlorite	–
3367-1509	2	589-651	631 ± 28	4	210–314	7

[a]Temperature in °C.
[b]Geothermometer from *Holland and Blundy* [1994].
[c]Geothermometer from *Cathelineau* [1988].
[d]N, number of calculations.

enhanced fluid flow occurred off-axis (e.g., during faulting and uplift into rift valley walls), we would expect to see chlorite overprinting higher-temperature assemblages that formed at the axis (e.g., similar to areas to the east and west), which was not observed.

We note that along the most easterly edge of the field area (i.e., eastern end of dives 3375 and 3367), there is an indication of a lateral change in alteration style in that $\delta^{18}O$ values decrease and samples in the basal sheeted dikes become chloritic (Figure 2b). This further illustrates the heterogeneity in alteration conditions within the sheeted dike complex and confirms that in this regard, many ophiolites are appropriate ancient analogues for studying crustal alteration patterns.

7.2. Area 1: A Fossil Discharge Zone?

We move our discussion now to the west where slightly younger crust exhibits very different alteration patterns (Figure 8c). Area 1 is characterized by a low $\delta^{18}O$ and Cu-depleted center that is hosted within massive sheeted dike outcrops very near the sheeted dike–volcanic transition. This 400-m-wide zone of sheeted dikes shows only minor rotation from the vertical and is cut by dike-parallel faults but is not fractured to the extent observed in area 2. The intact nature of these dikes and the ubiquitous but sparse distribution of very high temperature hydrothermal minerals suggest that this area was constructed by progressive dike injection without any significant periods of magmatic quiescence or enhanced tectonism [*Gillis*, 1995]. Each dike injection event would have caused a transient temperature fluctuation toward higher values (>500°C) in the wall rock, but the majority of the recorded fluid-rock interaction occurred at temperatures more typical of hydrothermal systems (~350°C).

Many alteration characteristics of the shallow sheeted dike complex in area 1 are indicative of a focused discharge zone that brought hot hydrothermal fluids to the seafloor. Compelling evidence for this interpretation comes from a study of hydrothermal fault breccias recovered along dive 2214 [*Saccocia and Gillis*, 1995]. These breccias are composed of metabasalt fragments cemented in a matrix of quartz, epidote, Mg-rich chlorite, chalcopyrite, and pyrite. Phase relationships and fluid inclusion data are consistent with formation from EPR-like vent fluids and the presence of Mg- rather than Fe-rich chlorite is attributed to the Fe/H_2S ratio of the vent fluids rather than entrainment of seawater in the subsurface [*Saccocia and Gillis*, 1995].

In order to further test this hypothesis we compare the mineralogical and geochemical characteristics of area 1 to those of

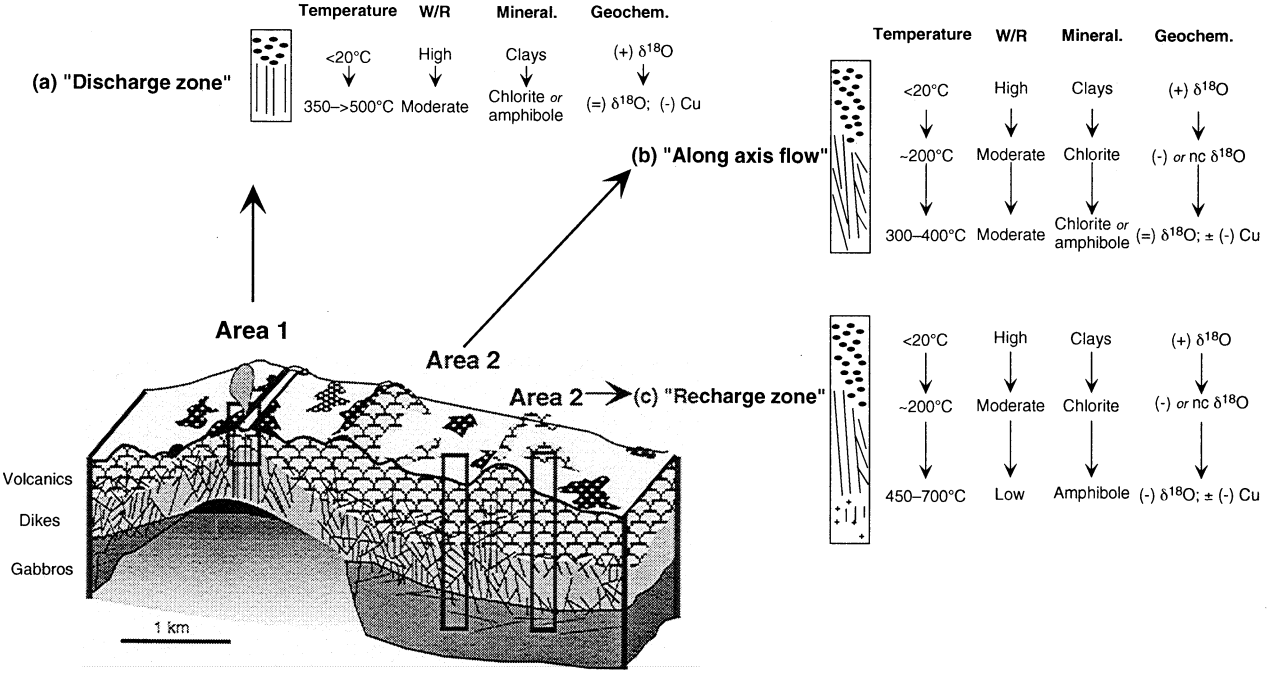

Figure 8. Schematic cross section of a segment of the EPR showing the relative positions of areas 1 (a) and 2 (b, c) in the near-axis environment and a summary of alteration characteristics and conditions prevalent in these areas. At the axis a melt lens (solid) underlies the volcanic and sheeted dike sequence, which in turn is underlain by crystal mush zone (light shading) (modified from *Karson et al.* [in press]). Abbreviations areW/R, water/rock ratios; Geochem., geochemical fluxes; (dashes), moderate loss; (equals), large loss; (pluses), moderate gain; nc, no change. See text for discussion.

discharge zones that are spatially associated with volcanic massive sulphide (VMS) deposits. Dikes in area 1 are not as pervasively altered as VMS-associated discharge zones but have similar mineral assemblages. A common assemblage associated with VMS discharge zones is chlorite, quartz, sulphides, and other phases [*Galley and Koski,* 1999]. Fe-rich chlorite is thought to be an important criterion for identifying discharge zones (e.g., Pitharokhoma [*Richards et al.*, 1989]; Turner-Albright [*Zierenberg et al.*, 1988]), whereas Mg chlorite is prevalent at Hess Deep. New chlorite solubility data, however, show that Fe chlorite does not reliably identify discharge zones as a variety of processes contribute to chlorite compositions [*Saccocia and Seyfried*, 1994]. *Saccocia and Seyfried* [1994] show, for example, that Mg-rich chlorite may be stabilized if precipitation of other phases (e.g., pyrite, epidote) causes fluid Fe/Mg ratios to decrease. Indeed, Mg chlorite is associated with the discharge zone for the active TAG hydrothermal mound where Sr isotopic data show that chloritic rocks formed by interaction with hydrothermal fluids with only a minor seawater component [*Honnorez et al.*, 1998; *Teagle et al.*, 1998]. Another similarity between the alteration in the dikes of area 1 and VMS-related discharge zones is the common replacement of plagioclase by quartz ± albite [e.g., *Honnorez et al.*, 1998; *Richards et al.*, 1989; *Zierenberg et al.*, 1988]. This assemblage is rare elsewhere in Hess Deep and very uncommon in oceanic metabasalts [e.g., *Gillis and Thompson*, 1993].

The term "discharge" generally calls to mind zones of high fluid flux where pervasively altered, chloritic basalts are cut by numerous quartz-sulphide veins [e.g., *Galley and Koski*, 1999]. In this regard, the sheeted dikes in area 1 do not resemble VMS-related discharge zones. Moreover, although whole rock $\delta^{18}O$ values are low, calculated water/rock ratios are lower than those typically expected for VMS deposits [e.g., *Alt and Teagle*, 1998]. These differences are likely related to the duration of the hydrothermal system driving fluid discharge. EPR deposits are small relative to those that form on ridges with slower spreading rates, are associated with seamounts, or are hosted in ophiolites [*Fouquet et al.*, 1996; *Hannington et al.*, 1998]. The life cycle of an EPR vent site is of the order of years to tens of years [*Von Damm*, 1995] whereas larger deposits evolved over much longer time periods (up to tens of thousands of years; e.g., TAG hydrothermal mound [*Humphris et al.*, 1995]). Hence we propose that the low $\delta^{18}O$ center in area 1 had insufficient time to evolve into chlorite-quartz-rich rocks typical of discharge zones associated with larger deposits.

7.3. Link With Spreading Axis

The complex geology of the region and the emplacement history of the rift shoulder block make it impossible to trace these exposures back to the EPR. However, on the basis of studies from other areas [see *Macdonald*, 1998], it is conceivable that magma supply was not constant during the construction of the crust exposed at the rift shoulder horst. In Figure 8 we show a schematic cross section of a fast spreading ridge [*Karson et al.,* 2001] that identifies the relative positions of areas 1 and 2 such that area 1 is under construction at the axis while area 2 is located 2–3 km off-axis. We speculate that area 1 was constructed during a period of high magma supply and that at some stage during its construction, hydrological and thermal conditions caused discharge to be focused in the shallow dikes for tens to a few hundreds of years (i.e., life cycle of EPR vent sites). Twenty to thirty thousand years earlier, when area 2 was being accreted at the axis, magmatism may not have been as robust. Evidence in support of this comes from the thick volcanic carapace [*Karson et al.,* 2001], localized but extensive brittle deformation [*Karson et al.,* 2001], and the absence of high-temperature discharge zones in the shallow dikes. While details of this scenario are largely unconstrained, this framework serves to illustrate how the spreading history of a fast spreading ridge segment can create significant lateral heterogeneity in fluid flow and alteration patterns.

8. Conclusions

Exposures of a volcanic sequence and sheeted dike complex over a 4-km-wide area at Hess Deep provide an ~60,000-year record of fluid-rock interaction for a section of crust that formed at the same segment along the fast spreading EPR. Mineralogical and geochemical characteristics and whole rock O isotope data for samples recovered along 14 submersible dive tracks reveal spatial heterogeneities on a spatial scale of hundreds of meters that has hitherto been unrecognized in modern oceanic crust. Within the sheeted dike complex, approximately one third of the scarp exposures show systematic mineralogical and geochemical changes with depth that are common in many ophiolites [e.g., *Harper et al.*, 1988] and comparable to Hole 504B [*Alt et al.*, 1996]. These changes are consistent with conventional models for recharge within axial hydrothermal systems in that temperatures and water/rock ratios increase and decrease, respectively, with depth. The specific characteristics of the basal sheeted dikes suggest formation during a less vigorous period of hydrothermal flow. In the central part of the field area, there is a narrow (≥400 m) zone within the basal sheeted dikes that shows the opposite trend, such that temperatures were lower and water/rock ratios higher than adjacent areas. We envision that this center of enhanced fluid flow formed at the axis during a period of tectonism that resulted in pervasive fracturing and dike rotation. A ≥400-m-wide discharge zone is exposed in the shallow sheeted dikes along the eastern margin of the field area. It is only in this area that there is field evidence for high-volume, high temperature fluid flow that can be linked to an EPR-like hydrothermal system.

The volcanic sequence is quite fresh, with minor oxidation and alteration to clay minerals, as would be expected for the young age of the field exposures (i.e., ~1.2 Ma). The most altered samples are enriched in K_2O, Rb, and $\delta^{18}O$ and were recovered from areas of intense fracturing. Whole rock oxygen isotope values are enriched but not to the extent of other well-studied volcanic sequences (e.g., Hole 504B), which is reflective of the young age of the crust.

Acknowledgments. J. Karson, E. Klein, and S. Hurst are thanked for inviting K.M.G. to participate in the 1999 Hess Deep cruise and for providing access to unpublished field data and interpretations. The geological relations presented here were derived from the careful observations of all the Hess Deep scientific party and were made possible by the expertise of officers and crew of the R/V *Atlantis* and the WHOI *Alvin* and DSL teams. We are grateful to L. Shi for his assistance with the microprobe analyses; P. Shanks for discussions about modeling isotopic systems; and M. Kohn (Associate Editor), R. Gregory, and C. Lécuyer for their thoughtful reviews. T. Gleeson participated in this project during a NSERC undergraduate research fellowship. This paper was prepared while K.M.G. was a Chercher Associaté at the CNRS-CRPG in Nancy, France. This project was supported by NSERC research grants to K.M.G. and K.M. and NSF grant 96-33725 (J. Karson, E. Klein, S. Hurst, PIs).

References

Agrinier, P., R. Hékinian, D. Bideau, and M. Javoy, O and H stable isotope compositions of oceanic crust and upper mantle rocks exposed in the Hess Deep near the Galapagos Triple Junction, *Earth Planet. Sci. Lett.*, *136*, 183-196, 1995.

Alexander, R.J., G.D. Harper, and J.R. Bowman, Oceanic faulting and fault-controlled subseafloor hydrothermal alteration in the sheeted dike complex of the Josephine ophiolite, *J. Geophys. Res.*, *98*, 9731-9759, 1993.

Alt, J.C., Subseafloor processes in mid-ocean ridge hydrothermal systems, in *Seafloor Hydrothermal Systems: Physical, Chemical, Biological, and Geological Interactions, Geophys. Monogr. Ser.*, vol. 91, edited by S.E. Humphris et al., pp. 85-114, AGU, Washington, D.C., 1995.

Alt, J.C., and D.A.H. Teagle, Probing the TAG hydrothermal mound and stockwork: Oxygen isotopic profiles from deep ocean drilling, *Proc. Ocean Drill. Progam Sci. Results*, *158*, 285-295, 1998.

Alt, J.C., J. Honnorez, C. Laverne, and R. Emmermann, Hydrothermal alteration of a 1 km section through the upper oceanic crust, Deep Sea Drilling Project Hole 504B: Mineralogy, chemistry, and evolution of seawater-basalt interactions, *J. Geophys. Res.*, *91*, 10,309-10,335, 1986a.

Alt, J.C., K. Muehlenbachs, and J. Honnorez, An oxygen isotopic profile through the upper kilometer of the oceanic crust, DSDP Hole 504B, *Earth Planet. Sci. Lett.*, *80*, 217-229, 1986b.

Alt, J.C., et al., Hydrothermal alteration of a section of upper oceanic crust in the eastern equatorial Pacific: A synthesis of results from Site 504 (DSDP Legs 69, 70, and 83, and ODP Legs 111, 137, 140, and148), *Proc. Ocean Drill. Progam Sci. Results*, *148*, 417-434, 1996.

Bailey, S.W., Chlorites: Structures and crystal chemistry, in *Hydrous Phyllosilicates (Exclusive of Micas)*, *Rev. Mineral.*, vol. 19, edited by S.W. Bailey, pp. 347-403, Mineral. Soc. of Am., Washington, D.C., 1988.

Baker, E.T., Y.J. Chen, and J. Phipps Morgan, The relationship between near-axis hydrothermal cooling and the spreading rate of mid-ocean ridges, *Earth Planet. Sci. Lett.*, *142*, 137-145, 1996.

Bettison, L.A., and P. Schiffman, Composition and structural variations of phyllosilicates from the Point Sal ophiolite, California, *Am. Mineral.*, *73*, 186-226, 1988.

Bevins, R.E., D. Robinson, and G. Rowbotham, Compositional variations in mafic phyllosilicates from regional low-grade metabasites and application of the chlorite geothermometer, *J. Metamorph. Geol.*, *9*, 711-721, 1991.

Bischoff, J.L., and F.W. Dickson, Seawater-basalt interaction at 200°C and 500 bars: Implication for origin of sea-floor heavy metal deposits and regulation of seawater chemistry, *Earth Planet. Sci. Lett.*, *25*, 385-397, 1975.

Bowers, T.S., and H.P. Taylor Jr., An integrated chemical and stable-isotope model of the origin of mid-ocean ridge hot spring systems, *J. Geophys. Res.*, *90*, 12,583-12,606, 1985.

Cathelineau, M., Cation site occupancy in chlorites and illites as a function of temperature, *Clay Mineral.*, *23*, 471-485, 1988.

Cathelineau, M., and D. Nieva, A chlorite solid solution geothermometer: The Los Azufres (Mexico) geothermal system, *Contrib. Mineral. Petrol.*, *91*, 235-244, 1985.

Clayton, R.N., and T.K. Mayeda, The use of bromine pentafluoride in the extraction of oxygen from oxides and silicates for isotopic analyses, *Geochim. Cosmochim. Acta*, *27*, 43-52, 1963.

Cole, D.R., and E.M. Ripley, Oxygen isotope fractionation between chlorite and water from 170 to 350°C: A preliminary assessment based on partial exchange and fluid/rock experiments, *Geochim. Cosmochim. Acta*, *63*, 449-457, 1998.

Craig, H., Standard for reporting concentrations of deuterium and oxygen-18 in natural waters, *Science*, *133*, 1833-1834, 1961.

Curewitz, D., and J.A. Karson, Geological consequences of dike intrusion at mid-ocean ridges, in *Faulting and Magmatism at Mid-Ocean Ridge Sprreading Centers, Geophys. Monogr. Ser.*, vol. 106, edited by W.R. Buck et al., pp. 117-136, AGU, Washington, D.C., 1998.

de Caritat, P., I. Hutcheon, and J.L. Walshe, Chlorite Geothermometry: A review, *Clays Clay Mineral.*, *41*, 219-239, 1993.

Elthon, D., J.R. Lawrence, R.E. Hanson, and C. Stern, Modeling of oxygen-isotope data from the Sarmiento ophiolite complex, Chile, in *Ophiolites and Oceanic Lithosphere*, edited by I.G. Gass, S.J. Lippard, and A.W. Shelton, *Geol. Soc. Spec. Publ.*, *13*, 185-197, 1984.

Epstein, S., and T. Mayeda, Variation of ^{18}O content of waters from natural sources, *Geochim. Cosmochim. Acta*, *4*, 213-224, 1953.

Fouquet, Y., R. Knott, P. Cambon, A. Fallick, D. Richard, and D. Desbruyers, Formation of large sulfide mineral deposits along fast spreading ridges: Example from off-axial deposits at 12°43'N on the East Pacific Rise, *Earth Planet. Sci. Lett.*, *144*, 147-162, 1996.

Francheteau, J., R. Armijo, J.L. Cheminee, R. Hékinian, P. Lonsdale, and N. Blum, 1 Ma East Pacific Rise oceanic crust and uppermost mantle exposed by rifting in Hess Deep (equatorial Pacific Ocean), *Earth Planet. Sci. Lett.*, *101*, 281-295, 1990.

Galley, A.G., and R.A. Koski, Setting and characteristics of ophiolite-hosted volcanogenic massive sulfide deposits, in *Volcanic-Associated Massive Sulfide Deposits: Processes and Examples in Modern and Ancient Settings*, edited by M.D. Hannington and C.T. Barry, pp. 215-236, Econ. Geol. Publ., Denver, Colo., 1999.

Gillis, K.M., Controls on hydrothermal alteration in a section of fast spreading oceanic crust, *Earth Planet. Sci. Lett.*, *134*, 473-489, 1995.

Gillis, K.M., and G. Thompson, Metabasalts from the Mid-Atlantic Ridge: New insights into hydrothermal systems in slow-spreading crust, *Contrib. Mineral. Petrol.*, *113*, 502-523, 1993.

Gregory, R.T., and H.P. Taylor, An oxygen isotope profile in a section of Cretaceous oceanic crust, Samail ophiolite, Oman: Evidence for $\delta^{18}O$ buffering of the oceans by deep (>5 km) seawater-hydrothermal circulation at mid-ocean ridges, *J. Geophys. Res.*, *86*, 2737-2755, 1981.

Hannington, M.D., A.G. Galley, P.M. Herzig, and S. Petersen, Comparison of the TAG mound and stockwork complex with Cyprus-type massive sulfide deposits, *Proc. Ocean Drill. Program Sci. Results*, *158*, 389-415, 1998.

Harper, G.D., J.R. Bowman, and R. Kuhns, A field, chemical, and stable isotope study of subseafloor metamorphism of the Josephine ophiolite, California-Oregon, *J. Geophys. Res.*, *93*, 4625-4656, 1988.

Haymon, R.M., D.J. Fornari, M.H. Edwards, S. Carbotte, D. Wright, and K.C. Macdonald, Hydrothermal vent distribution along the East Pacific Rise crest (9°09'-54'N) and its relationship to magmatic and tectonic processes on fast spreading mid-ocean ridges, *Earth Planet. Sci. Lett.*, *104*, 513-534, 1991.

Holland, T., and J. Blundy, Non-ideal interactions in calcic amphiboles and their bearing on amphibole-plagioclase thermometry, *Contrib. Mineral. Petrol.*, *116*, 433-447, 1994.

Honnorez, J.J., J.C. Alt, and S.E. Humphris, Vivisection and autopsy of active and fossil hydrothermal alterations of basalt beneath and within the TAG hydrothermal mound, *Proc. Ocean Drill. Program Sci. Results*, *158*, 231-254, 1998.

Hooft, E.E.E., R.S. Detrick, and G.M. Kent, Seismic structure and indicators of magma budget along the southern East Pacific Rise, *J. Geophys. Res.*, *102*, 27,319-37,340, 1997.

Humphris, S.E., et al., The internal structure of an active sea-floor massive sulphide deposit, *Nature*, *377*, 713-716, 1995.

Ishizuka, H., Mineral paragenesis of altered basalts from Hole 504B, ODP Leg 111, *Proc. Ocean Drill. Program Sci. Results*, *111*, 61-76, 1989.

Ito, E., and R.N. Clayton, Submarine metamorphism of gabbros from the Mid-Caymon Rise: An oxygen isotopic study, *Geochim. Cosmochim. Acta*, *47*, 535-546, 1982.

Karson, J.A., S.D. Hurst, and P. Lonsdale, Tectonic rotations of dikes in fast-spread oceanic crust exposed near Hess Deep, *Geology*, *20*, 685-688, 1992.

Karson, J.A., E.M. Klein, S.D. Hurst, C. Lee, P. Rivizzigno, D. Curewitz, and Hess Deep Scientific Party, Structure of uppermost fast-spread oceanic crust exposed at the Hess Deep Rift: Implications for subaxial processes at the East Pacific Rise, *Geochem. Geophys. Geosyst.*, in press, 2001.

Laverne, C., D.A. Vanko, P. Tararotti, and J.C. Alt, Chemistry and geothermometry of secondary minerals from the deep sheeted dike complex, Hole 504B, *Proc. Ocean Drill. Program Sci. Results*, *140*, 167-190, 1995.

Leake, B.E., et al., Nomenclature of amphiboles: Report of the Subcommittee on Amphiboles of the International Mineralogical Association, Commission on New Minerals and Mineral Names, *Am. Mineral.*, *82*, 1019-1037, 1997.

Lécuyer, C., and S. Fourcade, Oxygen isotope evidence for multi-stage hydrothermal alteration at a fossil slow-spreading center: The Silurian Trinity ophiolite (California, U.S.A.), *Chem. Geol.*, *87*, 231-246, 1991.

Lécuyer, C., and G. Gruau, Oxygen and strontium isotope compositions of Hess Deep gabbros (Holes 894F and 894G): High temperature interaction of seawater with the oceanic crust layer, *Proc. Ocean Drill. Program Sci. Results, 147*, 227-234, 1996.

Lécuyer, C., and B. Reynard, High-temperature alteration of oceanic gabbros by seawater (Hess Deep, Ocean Drilling Program Leg 147): Evidence form oxygen isotopes and elemental fluxes, *J. Geophys. Res.*, *101*, 15,883-15,897, 1996.

Lindsley, D.H., Pyroxene thermometry, *Am. Mineral.*, *68*, 477-493, 1983.

Liou, J.G., S. Kuniyoshi, and K. Ito, Experimental studies of the phase relations between greenschist and amphibolite in a basaltic system, *Am. J. Sci.*, *274*, 613-632, 1974.

Lonsdale, P., Structural pattern of the Galapagos microplate and evolution of the Galapagos Triple Junctions, *J. Geophys. Res.*, *93*, 13,551-13,574, 1988.

Lonsdale, P.F., Provenance and deformation of the volcanic section exposed at Hess Deep (abstract), *Eos Trans. AGU*, *80* (46), Fall Meet. Suppl., section F994, 1999.

Lowell, R.P., P. Van Cappellen, and L.N. Germanovich, Silica precipitation in fractures and the evolution of permeability in hydrothermal upflow zones, *Science*, *260*, 192-194, 1993.

Macdonald, K.C., Linkages between faulting, volcanism, hydrothermal activity, and segmentation on fast spreading centers, in *Faulting and Magmatism at Mid-Ocean Ridges, Geophys. Monogr. Ser.*, vol. 106, edited by R. Buck et al., pp. 27-58, AGU, Washington, D.C, 1998.

Manac'h, G., C. Lécuyer, and T. Juteau, A fluid inclusion and stable isotope study of hydrothermal circulation in a transform zone: Western Blanco Depression, northeast Pacific, *J. Geophys. Res.*, *104*, 12,941-12,969, 1999.

Manning, C.E., and D.K. Bird, Hydrothermal clinopyroxenes of the Skaergaard intrusion, *Contrib. Mineral. Petrol.*, *92*, 437-447, 1986.

Manning, C., P.E. Weston, and K.I. Mahon, Rapid high temperature metamorphism of the East Pacific Rise gabbros from Hess Deep, *Earth Planet. Sci. Lett.*, *144*, 123-132, 1996.

Matsuhisa, Y., J.R. Goldsmith, and R.N. Clayton, Oxygen isotopic fractionation in the system quartz-albite-anorthite-water, *Geochim. Cosmochim. Acta*, *43*, 1131-1140, 1979.

McCulloch, M.T., R.T. Gregory, G.J. Wasserburg, and H.P. Taylor Jr., Sm-Nd, Rb-Sr, and $^{18}O/^{16}O$ isotopic systematics in an oceanic crustal section: Evidence from the Samail ophiolite, *J. Geophys. Res.*, *86*, 2721-2735, 1981.

Moody, J.B., D. Meyer, and J.E. Jenkins, Experimental characterization of the greenschist/amphibolite boundary in mafic systems, *Am. J. Sci.*, *283*, 48-92, 1983.

Muehlenbachs, K., Alteration of the of the oceanic crust and the $\delta^{18}O$ history of seawater, in *Stable Isotopes in High Temperature Geological Processes, Rev. Mineral.*, vol. 16, edited by J.W. Valley, H.P. Taylor Jr., and J.R. O'Neil, pp. 425-444, Mineral. Soc. of Am., Washington, D.C., 1986.

Muehlenbachs, K., and R.N. Clayton, Oxygen isotope studies of fresh and weathered submarine basalts, *Can. J. Earth Sci.*, *2*, 172-184, 1972.

Nehlig, P., and T. Juteau, Deep crustal seawater penetration and circulation at ocean ridges: Evidence from the Oman ophiolite, *Mar. Geol.*, *84*, 209-228, 1988.

O'Neil, J.R., and H.P. Taylor Jr., The oxygen isotope and cation exchange chemistry of feldspars, *Am. Mineral.*, *52*, 1414-1437, 1967.

Richards, H.G., J.R. Cann, and J. Jensenius, Mineralogical zonation and metasomatism of the alteration pipes of Cyprus sulfide deposits, *Econ. Geol.*, *84*, 91-115, 1989.

Robinson, P., F.S. Spear, J.C. Schumacher, J. Laird, C. Klein, B.W. Evans, and B.L. Doolan, Phase relations of metamorphic amphiboles: Natural occurrence and theory, in *Amphiboles: Petrology and Experimental Phase Relations*, edited by P.H. Ribbe, pp. 1-211, Mineral. Soc. of Am., Washington, D.C., 1982.

Saccocia, P., and K.M. Gillis, Hydrothermal upflow zones in the oceanic crust, *Earth Planet. Sci. Lett.*, *136*, 1-16, 1995.

Saccocia, P.J., and W.E. Seyfried Jr., The solubility of chlorite solid solutions in 3.2 wt % NaCl fluids from 300-400°C, 500 bars, *Geochim. Cosmochim. Acta*, *58*, 567-585, 1994.

Saccocia, P.J., K. Ding, M.E. Berndt, J.S. Seewald, and W.E. Seyfried, Experimental and theoretical perspectives on crustal alteration at mid-ocean ridges, in *Alteration and Alteration Processes Associated With Ore-forming Systems, Short Course Notes*, vol. 11, edited by D.R. Lentz, pp. 403-432, Geol. Assoc. of Can., St. John's, Newfoundland, 1994.

Schiffman, P., and G.O. Fridleifsson, The smectite-chlorite transition in drillhole NJ-15, Nesjavellir geothermal field, Iceland: XRD, BSE and electron microprobe investigations, *J. Metamorph. Geol.*, *9*, 679-696, 1991.

Shanks, W.C., J.K. Bohlke, and R.R. Seal, Stable isotopes in mid-ocean ridge hydrothermal systems: Interactions between fluids, minerals, and organisms, in *Seafloor Hydrothermal Systems: Physical, Chemical, Biological, and Geological Interactions, Geophys. Monogr. Ser.*, vol. 91, edited by S.E. Humphris et al., pp. 194-221, AGU, Washington, D.C., 1995.

Stakes, D.S., and J.R. O'Neil, Mineralogy and stable isotope geochemistry of hydrothermally altered oceanic rocks, *Earth Planet. Sci. Lett.*, *57*, 285-304, 1982.

Stakes, D.S., and H.P. Taylor Jr., The northern Samail ophiolite: An oxygen isotope, microprobe, and field study, *J. Geophys. Res.*, *97*, 7043-7080, 1992.

Staudigel, H., S.R. Hart, and S.H. Richardson, Alteration of the oceanic crust: Processes and timing, *Earth Planet. Sci. Lett.*, *52*, 311-327, 1981.

Staudigel, H., T. Plank, B. White, and H.-U. Schimincke, Geochemical fluxes during seafloor alteration of the basaltic upper oceanic crust: DSDP Sites 417 and 418, in *Subduction: Top to Bottom, Geophys. Monogr. Ser.*, vol. 96, edited by G.E. Bebout et al., pp. 19-38, AGU, Washington, D.C, 1996.

Stewart, M.A., The geochemistry of dikes and lavas from Hess Deep: Implications for petrogenesis and magmatic crustal construction at fast spreading mid-ocean ridges and the stable-chlorine isotope geochemistry of mid-ocean ridge basalt glasses, Ph.D. thesis, Duke Univ., Durham, N. C., 2000.

Taylor, H.P., Jr., The oxygen isotope geochemistry of igneous rocks, *Contrib. Mineral. Petrol.*, *19*, 1-71, 1968.

Taylor, H.P., Jr., Water/rock interactions and the origin of H_2O in granite batholiths, *J. Geol. Soc. London*, *133*, 509-598, 1977.

Teagle, D.A.H., J.C. Alt, S.E. Humphris, and A.N. Halliday, Dissecting an active hydrothermal deposit: The strontium and oxygen isotopic anatomy of the TAG hydrothermal mound - whole rock and silicate minerals, in *Proc. Ocean Drill. Program Sci. Results*, *158*, pp. 297-309, 1998.

Thompson, G., Hydrothermal fluxes in the Ocean, in *Chemical Oceanography*, vol. 8, pp. 271-337, Academic, San Diego, Calif., 1983.

Velde, B., N. El Moutaouakkil, and A. Iijima, Compositional homogeneity in low-temperature chlorites, *Contrib. Mineral. Petrol.*, *107*, 21-26, 1991.

Von Damm, K., Controls on the chemistry and temporal variability of seafloor hydrothermal fluids, in *Seafloor Hydrothermal Systems: Physical, Chemical, Biological, and Geological Interactions, Geophys. Monogr. Ser.*, vol. 91, edited by S.E. Humphris et al., pp. 222-247, AGU, Washington, D.C., 1995.

Weston, P.E., Temperature, timing and fluid composition constraints for high temperature fracturing and hydrous mineral formation in gabbros from Hess Deep, M.Sc. thesis, Univ. of Calif., Los Angeles, 1998.

Wilcock, W.S.D., and J.R. Delaney, Mid-ocean ridge sulfide deposits: Evidence for heat extraction from magma chambers or cracking fronts?, *Earth Planet. Sci. Lett.*, *145*, 49-64, 1996.

Wolery, T.J., and N.H. Sleep, Hydrothermal circulation and geochemical flux at mid-ocean ridges, *J. Geol.*, *84*, 249-275, 1976.

Wood, B.J., and J.V. Walther, Rates of hydrothermal reactions, *Science*, *222*, 413-415, 1983.

Zheng, Y.F., Calculation of oxygen isotope fractionation in hydroxyl-bearing silicates, *Earth Planet Sci. Lett.*, *120*, 247-263, 1993.

Zierenberg, R.A., W.C. Shanks, III, W.E. Seyfried, Jr., R.A. Koski, and M.D. Strickler, Mineralization, alteration, and hydrothermal metamorphism of the ophiolite-hosted Turner-Albright sulfide deposit, southwestern Oregon, *J. Geophys. Res.*, *93*, 4657-4674, 1988.

K.M. Gillis and T. Gleeson, School of Earth and Ocean Sciences, University of Victoria, P.O. Box 3055, Victoria, British Columbia, Canada, V8W 3P6. (kgillis@uvic.ca)

J. Karson and M. Stewart, Division of Earth and Ocean Sciences, 103 Old Chemistry Building, Duke University, Durham, NC 27708-0230, USA. (jkarson@geo.duke.edu; mstewart@geo.duke.edu)

K. Muehlenbachs, Department of Earth and Atmospheric Sciences, University of Alberta, Edmonton, Alberta, Canada, T6G 2E3. (karlis.muehlenbachs@ualberta.ca)

(Received October 21, 2001; revised April 20, 2001;
accepted June 4, 2001.)